

To appear in *Astrophysical Journal*

## Nearby Supernova Factory Observations of SN 2005gj: Another Type Ia Supernova in a Massive Circumstellar Envelope.

The Nearby Supernova Factory

G. Aldering,<sup>1</sup> P. Antilogus,<sup>3</sup> S. Bailey,<sup>1</sup> C. Baltay,<sup>8</sup> A. Bauer,<sup>8</sup> N. Blanc,<sup>2</sup> S. Bongard,<sup>1,5</sup> Y. Copin,<sup>2</sup> E. Gangler,<sup>2</sup> S. Gilles,<sup>3</sup> R. Kessler,<sup>7</sup> D. Kocevski,<sup>1,6</sup> B. C. Lee,<sup>1</sup> S. Loken,<sup>1</sup> P. Nugent,<sup>1</sup> R. Pain,<sup>3</sup> E. Pécontal,<sup>4</sup> R. Pereira,<sup>3</sup> S. Perlmutter,<sup>1,6</sup> D. Rabinowitz,<sup>8</sup> G. Rigaudier,<sup>4</sup> R. Scalzo,<sup>1</sup> G. Smadja,<sup>2</sup> R. C. Thomas,<sup>1</sup> L. Wang,<sup>1</sup> B. A. Weaver<sup>1,5</sup>

### ABSTRACT

We report the independent discovery and follow-up observations of supernova 2005gj by the Nearby Supernova Factory. This is the second confirmed case of a “hybrid” Type Ia/IIn supernova, which like the prototype SN 2002ic, we interpret as the explosion of a white dwarf interacting with a circumstellar medium. Our early-phase photometry of SN 2005gj shows that the strength of the interaction between the supernova ejecta and circumstellar material is much stronger than for SN 2002ic. Our first spectrum shows a hot continuum with broad and narrow H $\alpha$  emission. Later spectra, spanning over 4 months from outburst, show clear Type Ia features combined with broad and narrow H $\gamma$ , H $\beta$ , H $\alpha$  and He I  $\lambda\lambda 5876, 7065$  in emission. At higher resolution, P Cygni profiles are apparent. Surprisingly, we also observe an inverted P Cygni profile for [O III]  $\lambda 5007$ .

---

<sup>1</sup>Physics Division, Lawrence Berkeley National Laboratory, 1 Cyclotron Road, Berkeley, CA, 94720

<sup>2</sup>Institut de Physique Nucléaire de Lyon, UMR5822, CNRS-IN2P3; Université Claude Bernard Lyon 1, F-69622 Villeurbanne France

<sup>3</sup>Laboratoire de Physique Nucléaire et des Hautes Energies IN2P3 - CNRS - Universités Paris VI et Paris VII, 4 place Jussieu Tour 33 - Rez de chaussée 75252 Paris Cedex 05

<sup>4</sup>Centre de Recherche Astronomique de Lyon, 9, av. Charles André, 69561 Saint Genis Laval Cedex

<sup>5</sup>University of California, Space Sciences Laboratory, Berkeley, CA 94720-7450

<sup>6</sup>Department of Physics, University of California, Berkeley, CA 94720

<sup>7</sup>Kavli Institute for Cosmological Physics, The University of Chicago, Chicago, IL 60637

<sup>8</sup>Department of Physics, Yale University, New Haven, CT 06250-8121

We find that the lightcurve and measured velocity of the unshocked circumstellar material imply mass loss as recently as 8 years ago. This is in contrast to SN 2002ic, for which an inner cavity in the circumstellar material was inferred. Within the context of the thin-shell approximation, the early lightcurve is well-described by a flat radial density profile for the circumstellar material. However, our decomposition of the spectra into Type Ia and shock emission components allows for little obscuration of the supernova, suggesting an aspherical or clumpy distribution for the circumstellar material. We suggest that the emission line velocity profiles arise from electron scattering rather than the kinematics of the shock. This is supported by the inferred high densities, and the lack of evidence for evolution in the line widths. Ground- and space-based photometry, and Keck spectroscopy, of the host galaxy are used to ascertain that the host galaxy has low metallicity ( $Z/Z_{\odot} < 0.3$ ; 95% confidence) and that this galaxy is undergoing a significant star formation event that began roughly  $200 \pm 70$  Myr ago. We discuss the implications of these observations for progenitor models and cosmology using Type Ia supernovae.

*Subject headings:* galaxies: abundances — stars: winds, outflows — supernovae: general — supernovae: individual (SN 2005gj, SN 2002ic)

## 1. Introduction

Type Ia supernovae (SNe Ia) are very important in astrophysics. As standardized candles they played the leading role in the determination that the mass-density of the Universe is sub-critical and that the expansion of the Universe is accelerating (Perlmutter et al. 1998; Garnavich et al. 1998; Riess et al. 1998; Perlmutter et al. 1999). They continue to play a major role in on-going efforts to determine the cause of this acceleration (Knop et al. 2003; Tonry et al. 2003; Riess et al. 2004; Astier et al. 2006) and in refining the determination of the Hubble constant (Riess et al. 2005). SNe Ia are a major source of chemical enrichment in galaxies, and may play a major role in the development of low-mass galaxies (e.g. Ferrara & Tolstoy 2000). For these many reasons, a long-standing goal has been to precisely identify the progenitor systems of SNe Ia. Of special interest for cosmology — where high-redshift SNe Ia are compared to low-redshift SNe Ia to deduce cosmological parameters — is the question of whether or not SNe Ia may arise from multiple channels (e.g., Howell 2001; Scannapieco & Bildsten 2005), acting on significantly different timescales, and in particular whether the relative contributions of multiple channels could act in such a way as to lead to biased cosmology results (Drell et al. 2000; Leibundgut 2001).

Historically speaking, the two most strongly favored SN Ia progenitor scenarios both involve the thermonuclear disruption of white dwarf stars (for an overview, see Branch et al. 1995). In the *single degenerate* model, a carbon-oxygen white dwarf accretes matter shed by a less-evolved companion star until it reaches the Chandrasekhar mass and explodes. The *double degenerate* scenario consists of the coalescence of a binary white dwarf system. The role of mass loss in the former scenario suggests an observational test to discriminate between the two models. The unambiguous detection of circumstellar hydrogen in the spectrum of a SN Ia would be interpreted as support for the single degenerate scenario. The search for this signature has resulted in mostly nondetections and upper limits on mass loss from the progenitor system, until recently.

The spectra of the peculiar SN Ia 2002ic (Wood-Vasey 2002; Hamuy et al. 2003) were the first to clearly reveal the interaction of the ejecta of one of these events with its circumstellar medium (CSM). The spectra of SN 2002ic resembled those of the spectroscopically peculiar, overluminous SN Ia 1991T, with features characteristic of a SN Ia though “diluted” (Hamuy et al. 2003). Most remarkably, these spectra exhibit narrow H $\alpha$  emission consistent with the redshift of the SN ( $z = 0.0667$ , Kotak et al. 2004) strongly reminiscent of SNe IIn (“n” for narrow hydrogen emission, Schlegel 1990). More circumstantial evidence obtained by comparing late time spectra of SNe IIn 1997cy and 1999E with SN 2002ic (Hamuy et al. 2003; Deng et al. 2004) suggests that some fraction of SNe IIn, ostensibly core-collapse SNe, may in fact be SNe Ia veiled by a substantial CSM.

Various interpretations of the observations of SN 2002ic have appeared in the literature. Motivated by the large mass inferred for the CSM, Hamuy et al. (2003) suggested that the progenitor system contained a massive asymptotic giant branch (AGB) star which shed the material prior to explosion. The AGB star could be a binary companion star, or the SN progenitor itself (a Type 1.5 SN, Iben & Renzini 1983). Most analyses agree that the density of the CSM was high, that a few tenths to several solar masses of material were shed, and that the mass loss rate was high or the CSM was clumpy (Kotak et al. 2004; Chugai et al. 2004c; Wang et al. 2004). Spectropolarimetry suggested that the geometry of the CSM was aspherical, and perhaps equatorially condensed (Wang et al. 2004; Uenishi et al. 2004). A light curve analysis (Wood-Vasey et al. 2004) implied a delay in the onset of the circumstellar interaction, suggesting that the mass loss phase had ended or trailed off in the years preceding the SN or that the inner CSM had been cleared by a fast wind, both consistent with the formation of a proto-planetary nebula (PPN; Kwok (1993)) by an AGB star.

Instead of an AGB scenario, Livio & Riess (2003) suggested that SN 2002ic was in fact the product of a double degenerate merger during the common envelope (CE) phase of a

binary; the white dwarf spirals in to coalesce with its companion’s core. However, the disk-like geometry and large radial extent of the CSM inferred from spectropolarimetry (Wang et al. 2004) and coalescence timescales that are incompatible with the timescale inferred for the mass ejection (Chugai & Yungelson 2004b) seem to rule out the CE coalescence model for SN 2002ic.

Motivated in part by the inferred presence of considerable CSM surrounding SN 2002ic, Wang (2005) advanced a hypothesis to explain the low values  $R_B \equiv A_B/E(B-V)$  often derived from observations of SNe Ia. Instead of the value  $R_B \sim 4.1$  expected for dust extinction in the Galaxy and LMC, values  $R_B \sim 2-3$  are often found (Tripp & Branch 1999; Phillips et al. 1999; Wang et al. 2003; Knop et al. 2003; Wang et al. 2005). In this hypothesis, dust in the immediate vicinity of the SN or at the highest velocities of its ejecta scatter SN light into the observer line of sight, thus adding back light and effectively reducing derived values of  $R_\lambda$  in the optical. The source of the dust may be a PN or PPN formed during the evolution of the progenitor system. This explanation suggests a continuum of models for ejecta-CSM interaction in SNe Ia. SNe Ia with more normal values of  $R_B$  could represent cases where the PN has had enough time to disperse into the host interstellar medium. Cases where  $R_B$  is low but there is no CSM interaction signature could occur in diffuse PNe. Still others (such as SN 2002ic) with a strong CSM interaction signature might originate in more compact PNe or PPNe.

Here we report on our observations of the recent SN 2005gj, which has much in common with SN 2002ic. Prieto et al. (2005) observed the development of spectral features characteristic of a SN Ia, during their follow-up of the discovery of SN 2005gj (Barentine et al. 2005; Frieman 2005), in what had originally appeared to be a SN IIn. The Nearby Supernova Factory (Aldering et al. 2002, SNfactory) had independently discovered SN 2005gj in images taken 2005 September 29, and acquired optical spectroscopy on 2005 October 3 which showed the strong, comparatively narrow Balmer  $H\alpha$  line that is the defining characteristic of the IIn class, and no visible SN Ia features. Both SN 2005gj and SN 2002ic were discovered by “blind” SN surveys (conducted without targeting specific galaxies) — SN 2005gj by the SDSS and the SNfactory, and SN 2002ic by the SNfactory prototype search (Wood-Vasey 2002). The two SNe are hosted by low-luminosity galaxies at about the same redshift, and their spectra at about 70 days after explosion are remarkably similar.

There are, however, important differences between the two events. Our earliest spectrum of SN 2005gj indicates a more intense, earlier interaction with the CSM than in the case of SN 2002ic. Additionally, the light curve of SN 2005gj is brighter than that of SN 2002ic, supporting the conclusion that the SN 2005gj ejecta-CSM interaction is stronger. Still, X-ray (Immler et al. 2005) and radio (Soderberg & Frail 2005) observations resulted in non-

detections, as was the case for radio observations of SN 2002ic (Berger et al. 2003; Stockdale et al. 2003).

The organization of this paper is as follows. In §2 we present new photometry and spectroscopy of SN 2005gj covering numerous epochs extending more than four months past the explosion date. We also describe spectroscopic observations of the host galaxy. In §3 we analyze the SN 2005gj observations in the context of a two-component SN plus CSM interaction model in order to place constraints on the amount of CSM and the relative contributions of SN and CSM light to the observations. §4 presents an analysis of the host galaxy spectroscopy and photometry. These are brought together in §5 in a discussion of our results and their possible implications for SN progenitor systems and cosmology. §6 summarizes our findings. We take  $H_0 = 70 \text{ km s}^{-1} \text{ Mpc}^{-1}$  throughout this paper.

## 2. Data

### 2.1. Photometry

#### 2.1.1. Search, Discovery, and Follow-up

The SNfactory independently discovered SN 2005gj (our SNF20050929-005) on 2005 September 29.45 UCT (JD 2453642.95) in wide-field images obtained using the QUEST-II CCD camera (Rabinowitz et al. 2003) on the Samuel Oschin 1.2m telescope on Mount Palomar, CA, in collaboration with the JPL Near-Earth Asteroid Tracking (NEAT) component of the Palomar-QUEST Consortium. These asteroid and SN search images consist of 60 second exposures in an RG610 filter. Each field is visited three times within an hour in order to detect the motion of asteroids (which we reject) and eliminate cosmetic defects. Subsequent to discovery, additional images of SN 2005gj were obtained by NEAT, as well as by the QUEST collaboration. QUEST images were obtained in drift-scan mode, using either Johnson  $U, B, R, I$  filters or Gunn  $r, i, z$  filters.

The images are transferred from Mount Palomar to the High Performance Storage System (HPSS) at the National Energy Research Scientific Computing Center (NERSC) in Oakland, CA via the wireless HPWREN network<sup>1</sup> and the ESnet network.<sup>2</sup> These images are processed using the Parallel Distributed System Facility (PDSF) at NERSC. The first level of processing decompresses the images, subtracts an average bias image, and divides by a normalized

---

<sup>1</sup>Information on HPWREN (PI: H.-W. Braun) is available at <http://hpwren.ucsd.edu>.

<sup>2</sup>Information on the US Department of Energy's ESnet is available at <http://www.es.net>.

median sky flat image constructed from images taken around the same time on the same night. An object-finding algorithm identifies objects that have counterparts in the USNO-A1.0 POSS-E catalog (Monet et al. 1996), and these matches are used to determine the image astrometry.

Images of a given field taken on the same night are spatially aligned, convolved to a point spread function (PSF) common to these images and their reference images, scaled in flux, and coadded to form a new image. For NEAT images, archived unfiltered NEAT images from 2001-2003 are used as references. For QUEST drift-scan images, references are taken from QUEST drift-scan runs in 2003 and 2004. Reference images covering the same field are astrometrically aligned to match the new images, PSF convolved, then coadded. This reference sum is then scaled and subtracted from the new images. Residual sources passing a set of image parameter cuts are automatically identified and passed on to human scanners for final confirmation.

### 2.1.2. Photometry and Lightcurve

For consistency in the analysis, the NEAT data were reprocessed using the same 5 reference images for all new images. For each night, the photometry of one of the new images was calibrated against SDSS  $i$  magnitudes (Adelman-McCarthy et al. 2006) for stars on that image. Between 90 and 199 stars were used, depending upon the observing conditions each night. Aperture photometry for each non-saturated star on the image was compared to the SDSS  $i$  magnitude and an image zeropoint was fit, including  $(r-i)$  and  $(i-z)$  color corrections to account for the differences between the RG610, Johnson  $I$ , or Gunn  $i$ , and SDSS  $i$  filters. All other images used in the subtraction were photometrically calibrated against this new image.

Aperture photometry was performed on SN 2005gj using these zeropoints to produce magnitudes calibrated to the SDSS  $i$  band. The color of SN 2005gj was interpolated from QUEST drift-scan images taken in several filters, or from our spectrophotometry (see §2.2). Additionally, flux calibrated SNIFS spectra, described in §2.2.1, were used to synthesize  $i$  magnitudes and  $(r-i)$  and  $(i-z)$  colors on the SDSS system for dates JD-2453000 of 647.09, 699.96, 706.96, and 706.98.

SN 2005gj was not evident on images taken (under poor weather conditions) on 2005 September 23.4. IRAF<sup>3</sup> aperture photometry of the subtracted image at the location of

---

<sup>3</sup>IRAF is distributed by the National Optical Astronomy Observatories, which are operated by the

SN 2005gj was used to establish that a  $2\sigma$  upward fluctuation of the background would have corresponded to an object having  $i = 20.15$ . Therefore we quote this as the limiting magnitude for SN 2005gj on that day.

Observing conditions on 2005 November 18.4 were cloudy and there were an insufficient number of stars on the image to perform the necessary astrometric and PSF matching needed for our automated subtraction pipeline. Instead, these images were individually processed with IRAF using 5 nearby stars to determine the magnitude zeropoint. The errors on the 2005 November 18 photometry measurements are dominated by the large sky background.

To compare with SN 2002ic  $V$ -band data and models, SN 2005gj  $V$ -band magnitudes were estimated using extrapolations from Johnson  $B$ , Johnson  $R$ , Gunn  $r$ , and RG610 filters, using the shape of the SNIFS spectra for color corrections. Nights on which we have QUEST data in multiple filters confirms that this extrapolation method produces photometry results consistent within the stated uncertainties. When available, SNIFS spectra were also used to synthesize  $V$ -band photometry.

Table 1 lists the measured  $i$  photometry and Table 2 lists the derived  $V$  photometry. Correction for Galactic extinction, which in the direction of SN 2005gj is  $E(B-V) = 0.121$  ( $A_B = 0.52$  mag) according to the maps of Schlegel et al. (1998), has not been applied in these tables. Figure 1 illustrates our lightcurve data, including Galactic extinction corrections. Photometry points for SN 2002ic are overplotted for comparison (Hamuy et al. 2003; Wood-Vasey et al. 2004). The SN 2002ic points have been extinction corrected and adjusted to account for cosmological effects arising from the (small) difference in redshift (0.0667 vs. 0.0616, see §2.2.2). No adjustment for redshift-dependent bandpass differences has been made, since this effect is negligible for these filters and this redshift difference.

The assigned magnitude uncertainties are predominantly from the dispersion measured for the zeropoint calibration, which includes statistical uncertainties arising from Poisson fluctuations as well as residual errors from flat fielding, fringing, etc. The QUEST images taken with the Johnson  $I$  filter also had significant color correction terms (0.250 and 0.285), which combined with the color uncertainty of SN 2005gj for those dates contributed several hundredths of a magnitude to the uncertainty.

A quadratic fit to the flux on the first 40 days implies an explosion date of JD 2453636.1 (2005 September 22.6 UTC), slightly before our upper limit of  $i < 20.15$  on September 23.4. In §3.1 we will use a CSM interaction model to refine this estimate.

## 2.2. Optical Spectroscopy

Our discovery of SN 2005gj on 2005 September 29.45 UTC prompted our follow-up confirmation spectroscopy on 2005 October 3.59 UTC (JD 2453647.09). We obtained additional optical spectroscopy at multiple epochs spanning four months after explosion. Here we detail the spectroscopic reductions and describe the major features observed. Table 3 provides technical details of these observations.

### 2.2.1. SNIFS Spectroscopy

Observations of SN 2005gj were obtained with the SuperNova Integral Field Spectrograph (SNIFS, Aldering et al. 2002; Lantz et al. 2004), operated by the SNfactory. SNIFS is a fully integrated instrument optimized for automated observation of point sources on a diffuse background over the full optical window at moderate spectral resolution. It consists of a high-throughput wide-band pure-lenslet integral field spectrograph (IFS, “à la TIGER,” Bacon et al. 1995, 2000, 2001), a multi-filter photometric channel to image the field surrounding the IFS for atmospheric transmission monitoring simultaneous with spectroscopy, and an acquisition/guiding channel. The IFU possesses a fully filled  $6'' \times 6''$  spectroscopic field-of-view subdivided into a grid of  $15 \times 15$  spatial elements (spaxels), a dual-channel spectrograph covering 3200–5200 Å and 5100–11000 Å simultaneously, and an internal calibration unit (continuum and arc lamps). SNIFS is permanently mounted on the south bent-Cassegrain port of the University of Hawaii 2.2-m telescope (Mauna Kea), and is operated remotely. The SNIFS spectra of SN 2005gj were reduced using our dedicated data-reduction procedure, similar to that presented in § 4 of Bacon et al. (2001). Here we briefly outline the process.

After standard CCD preprocessing and subtraction of a low-amplitude diffuse-light component, the 225 spectra from the individual lenslets of each SNIFS exposure were extracted from each blue and red spectrograph exposure, and re-packed into two  $(x, y, \lambda)$ -datacubes. This highly specific extraction is based upon a detailed optical model of the instrument including interspectrum crosstalk corrections. The datacubes were then wavelength-calibrated, using arc lamp exposures acquired immediately after the science exposures, and spectro-spatially flat-fielded, using continuum lamp exposures obtained during the same night. Cosmic rays were detected and corrected using a 3D-filtering scheme applied to the datacubes.

SN and standard star spectra were extracted from the 225 spaxels,  $s$ , of each  $(x, y, \lambda)$ -datacube using a wavelength-dependent Gauss-Newton PSF fit method by minimizing  $\chi^2$ . The adopted PSF model is

$$\text{model}(s, \lambda) = S_{\text{SN}}(\lambda) \cdot I_{\text{PSF}}(s, \vec{x}_{\text{SN}}(\lambda_{\text{ref}}), \lambda, \dots) + C(\lambda) \quad (1)$$

where  $S_{\text{SN}}$  is the supernova spectrum,  $I_{\text{PSF}}$  is the PSF integrated over one spatial element, and  $C(\lambda)$  is a spatially uniform background distribution. Free parameters include the position of the SN at an arbitrary reference wavelength (the position at other wavelengths follows an atmospheric differential refraction function; see Filippenko 1982), the position angle of the microlens array on the sky, the SN spectrum, the background distribution, and the input parameters for the chosen PSF (seven in our case, not including the SN position). Uncertainties used in the  $\chi^2$  minimization incorporate the detector gain and readout noise in the calculation of the detector and photon noise.

The PSF is modeled as a weighted sum of two bidimensional Gaussians designed to account for variation near both the core and wings. The FWHM of each Gaussian is wavelength dependent, going as  $\lambda^\gamma$ . Fit parameters include the orientation angle of the elliptical Gaussians, the FWHMs at one arbitrary wavelength for each Gaussian, two  $\gamma$  values, and a relative scaling between the Gaussians.

An attenuation estimate for each exposure was made using the stars observed by the SNIFS multifilter photometric channel. Objects in the field (spatially subdivided into five regions each monitoring a different wavelength range) were detected using SExtractor (Bertin & Arnouts 1996), and their fluxes measured using an adapted version of the Supernova Legacy Survey aperture photometry code, Poloka. For the objects that were matched over all nights, the fluxes in each filter were summed, giving a total flux per filter per night. These fluxes were then normalized by the flux on a specific night considered photometric, allowing us to make an estimation of the relative flux extinction in each filter band for the observations on non-photometric nights. Seeing and the stability of the atmospheric transmission were assessed using SNIFS guider video frames acquired during our exposures.

Variable cloud conditions prevailed on the night of 2005 October 3 UTC. The multi-filter transmission measurement indicates an average (gray) correction factor of  $3.74 \pm 0.09$ . Conditions on the night of November 25 were photometric. The night of December 2 was not photometric, however, an average transmission correction of  $1.01 \pm 0.01$  was derived from the multifilter, indicating that conditions were mostly clear at the time SN 2005gj was observed. These correction factors are applied to the spectra when synthesizing magnitudes and measuring line luminosities.

The final flux-calibrated spectra appear in Figure 2. From the top, the first, second and fourth spectra were acquired with SNIFS. The wavelength range displayed corresponds to the region where we are most confident in the calibration and extraction. In particular, the region surrounding the dichroic has been removed for clarity, as the signal-to-noise here is low and is not always properly treated in the current reduction pipeline. The flux solution is conservatively estimated to be accurate to within 5% on November 25 and December 2,

but perhaps only 10-15% on October 3. These limits are imposed by the simplified flux calibration procedure used here, in which no attempt has been made to derive an independent atmospheric extinction curve for the nights observed, but where a standard Mauna Kea atmospheric extinction curve (Beland, Boulade, & Davidge 1998) has been adopted. A full calibration solution for each night is still in development.

Initial spectroscopy was obtained 4 days after our discovery. As Figure 2 shows, at this early phase SN 2005gj resembled a SN IIn (a featureless continuum punctuated by a strong, narrow H $\alpha$  emission feature), rather than a SN Ia that the SNfactory normally would have continued to follow. Later SNIFS spectra reveal the continued presence of the H $\alpha$  feature. In the day 64 spectrum we also detect a weak emission feature due to He I  $\lambda$ 5876. On day 71 we also detect He I  $\lambda$ 7065. Broad features, attributable to an underlying SN at about a month after maximum, include Ca II H&K and infrared triplet, and absorption from Fe III at 4700 Å and 5400 Å. In these spectra there is no detectable Na I D absorption to indicate reddening by the host galaxy.

### 2.2.2. Keck Spectroscopy

We first observed SN 2005gj on the Keck I telescope on 2005 December 2.3 UTC using the Low Resolution Imaging Spectrograph (LRIS Oke et al. 1995). The spectrograph was configured with the 5000 Å blaze, 300 l/mm grism in the blue channel, and the 8500 Å blaze, 400 l/mm grating in the red channel. A dichroic with crossover at 6800 Å was used to separate the light into red and blue channels, as the primary science that night targeted high-redshift SNe. Conditions were non-photometric during this part of the night — prior to the clear conditions that prevailed later when our SNIFS spectrum was obtained — and seeing varied between 0''.7 and 1''.0. A 900 sec integration using a 1'' wide slit was obtained, with a position angle of 0° in order to pass through both the SN and its apparent host galaxy. Data were taken at airmass 1.08, making corrections for atmospheric differential refraction negligible.

The data were overscan-subtracted, bias-subtracted, flat-fielded using internal lamp exposures, wavelength-calibrated, and extracted using standard IRAF procedures. The wavelength calibration arcs were obtained at the beginning the night; since LRIS suffers from flexure, the wavelength zeropoints were adjusted for each spectrum using the night sky lines referenced to the high resolution night sky spectrum of Hanuschik (2003). Flux calibration and telluric feature removal was performed using the standard stars BD+174708, Feige 34, Feige 67, Feige 110, and HZ 44. For blue standard stars, the 6000-6800 Å region of the blue channel spectrum shows contamination by second-order light. This was accounted for when

determining the flux correction, and we find good agreement in the shape of the SN 2005gj spectrum between the blue and red channels over the 6620–6770 Å region where they overlap. A standard Mauna Kea atmospheric extinction curve (Beland, Boulade, & Davidge 1998) was assumed, since non-photometric conditions precluded a direct determination of the extinction. The resulting spectrum of SN 2005gj is shown in Figure 2. The S/N ratio of the spectrum is 100 or greater per 1.43 Å pixel over the range 4000–9000 Å.

While correction for atmospheric differential refraction is unimportant for this spectrum, since atmospheric seeing is wavelength dependent the amount of light lost at the LRIS slit also depends on wavelength. This effect is important for slit-widths comparable to the seeing — as with these observations — and its incorporation into the flux calibration is very dependent on the seeing and mis-centering experienced by the standard stars relative to that experienced by the target. As SNIFS does not suffer from this effect, we defer to the SNIFS spectrum taken this same night when performing fits to the flux over a long wavelength baseline.

The full 2D LRIS spectrum shows narrow H $\alpha$  extending along the major axis of the host galaxy. From this narrow emission we measure a host galaxy heliocentric redshift of  $0.0616 \pm 0.0002$ . The peak of the narrow emission from SN 2005gj is redshifted with respect to the host by  $90 \pm 50$  km/s. In addition to the spectrum of SN 2005gj, a region of the host galaxy located 3''.4 south of SN 2005gj, showing strong H $\alpha$  emission and relatively free from contamination by SN 2005gj, was extracted from the LRIS red channel. This spectrum is analyzed in §3.2

As in the SNIFS spectrum, H $\alpha$ , He I  $\lambda 5876$ , and He I  $\lambda 7065$  are visible in emission from SN 2005gj. In addition, H $\beta$  emission is clearly seen in the LRIS spectrum, and has a shape consistent with that seen in H $\alpha$ . H $\gamma$  is also detected, but H $\delta$  is not. With the higher resolution used for the LRIS spectrum, P Cygni profiles are apparent in the H $\alpha$  and H $\beta$  lines. He I  $\lambda 4471$  and He I  $\lambda 6678$  are not detected either in emission or absorption. Weak (equivalent width  $EW \sim 0.4$ –0.7 Å), unresolved H9, H8, and Ca II H&K/He are detected in absorption. Na I D absorption from the Galaxy is detected, having  $EW = 0.6$  Å from the sum of the (unresolved) D<sub>1</sub> and D<sub>2</sub> components; Na I D absorption at the host galaxy redshift is not detected in this spectrum. Rather, at this location there appears to be either a flat-topped high-velocity red tail associated with He I  $\lambda 5876$  or else a complex combination of Na I D emission plus absorption, similar to that seen for SN 1994W by Chugai et al. (2004a). Also of interest is an inverted P Cygni profile in [O III]  $\lambda 5007$ .

SN 2005gj was observed a second time with LRIS, on 2006 February 2.2 UTC, using the 4000 Å blaze, 600 1/mm grism in the blue and the 7500 Å blaze, 1200 1/mm grating in the blue. This set-up allowed us to obtain the higher resolution required to better examine the

shapes of the  $\text{H}\beta$  and  $\text{He I } \lambda 5876$  emission lines and higher level Balmer absorption lines, and to search for  $\text{Na I D}$  absorption indicative of host-galaxy extinction. The night was clear, and the seeing was  $0''.9$  for this 900 sec exposure. Processing followed the steps described for 2005 December 2, except that in this case the flux calibration was obtained using G191B2B.

The blue Keck LRIS spectrum is remarkably similar to the spectrum taken two months earlier. The Balmer series from  $\text{H}\delta$  up to the Balmer limit is clearly seen in absorption in this spectrum.  $\text{H}\beta$  and  $\text{H}\gamma$  show clear P Cygni profiles, while  $\text{H}\delta$ ,  $\text{H}\epsilon$ , and  $\text{H}\delta$  show strong absorption but only a hint of emission. The absorption of the strong Balmer absorption lines and  $\text{Ca II H}$ , appear asymmetric, with enhanced wings on the blue side. The inverted P Cygni profile for  $[\text{O III}] 5007\text{\AA}$  is also much more clear. The blue spectrum also exhibits narrow  $[\text{O II}] \lambda\lambda 3727, 3729$ , most likely from the host galaxy. These lines are shown in Figure 4.

In the higher resolution red spectrum  $\text{He I } \lambda 5876$  clearly exhibits a P Cygni profile. This is modeled in §3.2. In addition, very little  $\text{Na I D}$  absorption from the host can be detected. The derived absorption is  $\text{EW}(\text{D1}) = 0.16 \text{ \AA}$  and  $\text{EW}(\text{D2}) = 0.12 \text{ \AA}$ . These values are sensitive to the setting of the “continuum” level, which in this case is comprised of the broad component of  $\text{He I } \lambda 5876$  (see §3.2). We note that these lines require a slightly smaller redshift,  $z=0.0613$ , within the uncertainty quoted for the redshift determination from December 2. However, it is possible that these lines arise from material approaching by  $\sim 90 \text{ km s}^{-1}$ . There is some hint that these weak absorption features could be due to P Cygni profiles associated with  $\text{Na I D}$  from the CSM. Galactic  $\text{Na I D}$  is also detected quite clearly. We measure  $\text{EW}(\text{D1}) = 0.41 \text{ \AA}$  and  $\text{EW}(\text{D2}) = 0.30 \text{ \AA}$ ; the total of  $0.7 \text{ \AA}$  is slightly higher than that measured on December 2, probably due to resolution effects.

### 3. Analysis

#### 3.1. Lightcurve Fits

Figure 3 shows a comparison between SN 2005gj, SN 2002ic, and SN templates in Johnson  $V$  and SDSS  $i$  filters. The SN templates used are new versions of templates discussed in Nugent et al. (2002).<sup>4</sup> The templates are scaled so that  $M_B^{\text{peak}} = -19.5$  for the Branch-normal case and  $M_B^{\text{peak}} = -19.86$  in the SN 1991T-like template (Saha 2001). In  $V$ -band, the SN 2005gj points are synthesized photometry from SNIFS observations, as well as values interpolated or extrapolated using NEAT and QUEST data in other bands. The  $i$ -band

---

<sup>4</sup>[http://supernova.lbl.gov/~nugent/nugent\\_templates.html](http://supernova.lbl.gov/~nugent/nugent_templates.html)

points include NEAT and QUEST photometry measurements as well as synthesized photometry from SNIFS. For comparison, we again show the corresponding  $V$  photometry for SN 2002ic. In order to understand the SN 2005gj lightcurve, we briefly review the modeling that has already been performed for SN 2002ic.

Using only the Hamuy et al. (2003) SN 2002ic  $BVI$  data for SN 2002ic, Chugai & Yungelson (2004b) found that a flat CSM radial density profile was needed to fit the data around 60 and 80 days after explosion. Uenishi et al. (2004) found that  $\rho \propto r^{-1.8}$  was needed once the late-time SN 2002ic photometry from Deng et al. (2004, ; not shown) was included. An updated model by Chugai et al. (2004c) inferred the presence of a flat density profile out to  $3 \times 10^{15}$  cm, followed by a  $\rho \propto r^{-1.4}$  fall off. For this model it was noted that SN Ia-CSM interactions will have a much more efficient conversion of kinetic energy to luminosity than a SN IIn due to the substantially higher X-ray opacity from Fe-group elements in the SN Ia envelope (Chugai et al. 2004c). Wood-Vasey et al. (2004) added several early-time photometry points, additional late-time photometry, and photometry that better separated the SN lightcurve from a later bump due to the CSM interaction. They found reasonable agreement with the data using the fainter SN 1991T-like template from Nugent et al. (2002), a CSM density profile of  $\rho \propto r^{-2}$ , and a constant kinetic energy to luminosity conversion term for the CSM interaction (Chevalier & Fransson 1994), provided that the SN ejecta did not interact with the CSM until around 8 days after the explosion. A more generalized — but non-unique — density profile with excess material for the second bump was able to fit all the data; however, an early gap was still required (Wood-Vasey et al. 2004).

SN 2005gj is significantly brighter than either SN 2002ic or the SN templates, indicating a much stronger and earlier CSM interaction. Therefore, unlike SN 2002ic, no decline after SN maximum light is seen. Over the time period for which we have SN 2005gj data, the Chugai & Yungelson (2004b) model with a flat density profile matches reasonably well in  $i$ -band, as shown in Figure 5. However, this model declines too quickly in  $V$ -band. The best fit in  $i$ -band is obtained with an explosion date of 2005 September 20.4, which is 2.2 days prior to the estimation from a simple second order polynomial fit to the rise of the lightcurve.

Our first spectrum is from JD 2453647.09, which is 11 days after explosion for an explosion date of September 22.6. The expected fraction of SN light on that day is sensitive to the assumed explosion date —  $29.1_{-20.2}^{+14.3}\%$  in  $i$ -band and  $24.6_{-14.2}^{+11.5}\%$  in  $V$ -band — where the quoted uncertainties are determined by adjusting the assumed explosion date between September 18.6 and September 24.6. On later dates for which we have spectra the uncertainty due to the explosion date is much smaller. For 64 and 71 days after explosion the SN 1991T-like lightcurve template comparison implies  $i$ -band SN Ia contributions of  $16.7_{-1.7}^{+2.3}\%$  and

$12.2_{-1.2}^{+2.4}\%$ , respectively. In  $V$ -band these percentages are  $14.9_{-1.6}^{+4.7}\%$  and  $14.9_{-1.0}^{+2.1}\%$ . The quoted uncertainties do not include uncertainties in the lightcurve template itself.

If there were a gap between the SN Ia and the inner CSM radius interaction, as found by Wood-Vasey et al. (2004) for SN 2002ic, the SN Ia explosion could have occurred as early as September 15.9 based upon the lightcurve data alone. However, the SN light fractions derived from spectral decomposition in §3.2 imply a SN Ia explosion date later than September 22.6. (As noted below, the radiation field from the shock may modify the spectrum within the SN photosphere at early times.) For the purposes of this paper, we consider September 18.6 to 24.6 to be a conservative range of possible explosion dates.

### 3.2. Spectral Analysis

Our first spectrum, shown at the top of Figure 2, was observed 4 days after our discovery or 11 days after explosion, using the outburst date of September 22.6 derived in §2.1.2. This is the earliest spectrum of any confirmed (SN 2002ic) or suspected (SN 1997cy or SN 1999E) SN Ia+CSM event. This initial spectrum of SN 2005gj is indistinguishable from that of a classical SN IIn. The only structure visible is the narrow H $\alpha$  emission superimposed on a broader component; there is no obvious indication of any feature typically associated with a SN Ia spectrum.

Our later spectra, also in Figure 2, agree almost feature-for-feature with the spectra of SN 2002ic at about the same phase. Figure 6 illustrates the overall similarity of the combined SNIFS spectrum obtained 2005 December 2.5 (71 days after explosion) with the 2003 January 3 spectrum of SN 2002ic. A few differences are evident in this comparison. The spectrum of SN 2005gj possesses an emission peak at 4000 Å while that of SN 2002ic does not. Also, the absorption notch on the blue side of the emission hump at 5500 Å clearly visible in SN 2002ic is much more subtle in SN 2005gj.

In their analysis of SN 2002ic, Hamuy et al. (2003) remark on the similarity of their spectra to that of a SN Ia with “diluted” spectral features, and decompose their spectra in terms of a SN Ia component plus a smoothly-varying continuum. This simple type of spectrum decomposition in the case of SN+CSM interaction is not strictly correct, since it neglects radiative coupling between the CSM interaction and line-forming regions (Branch et al. 2000; Chugai et al. 2004c). The CSM interaction region illuminates the SN envelope from without and “mutes” the SN features. P Cygni profiles lose contrast and may even invert, depending on details of the CSM interaction such as luminosity and geometry. A more detailed model of the formation of the SN spectrum including the effects of this coupling

would help constrain the effects of muting, and also provide insight into the geometry of the interaction region itself. Still, a simple linear decomposition of SN 2005gj may constrain the SN contribution in the SDSS *i*-band flux where SN Ia spectrum formation is less directly influenced by line opacity (Pinto & Eastman 2000).

After applying a Galactic extinction correction of  $E(B-V) = 0.121$ , we decompose the SNIFS spectra of SN 2005gj using a SN 1991T-like spectral template (Nugent et al. 2002) and a smoothly-varying function of wavelength to represent the CSM. The spectroscopically normal SN Ia template does not account for the SN features as well as the SN 1991T-like template. The CSM contribution in the earliest spectrum is modeled as a blackbody, and in the later spectra as a low-order polynomial. Using a blackbody at late time produces a less satisfactory fit than the polynomial. The decompositions appear in Figure 7.

In Figure 7a, we present the day 11 spectrum decomposed into a 12,400 K blackbody plus SN 1991T-like spectrum 10 rest-frame days after explosion. The derived ratio of the SN Ia template to total *i*-band flux is 20%. Thus, despite the superficial resemblance to a SN IIn, SN 2005gj does show subtle but significant evidence for SN Ia spectral features. In fact the amount of SN light inferred from the linear decomposition is consistent with the prediction made in §3.1. This self-consistency suggests that at most a small fraction of the SN photosphere can be obscured by the CSM.

Decompositions of the later-time SNIFS spectra appear in Figures 7b and 7c. We have adopted template spectra at rest frame phases of 60 and 66 days after explosion for the observations on November 25.5 and December 2.5, respectively. On both epochs, the SN 1991T-like+CSM superposition exhibits a flux deficit at 5400 Å relative to the observed spectrum. This absorption is the same robust notch observed in the spectrum of SN 2002ic. In their analysis of the spectrum of SN 1991T, Mazzali et al. (1995) attribute this absorption to Fe II  $\lambda 5535$  but do not fit it. A lower iron abundance relative to SN 2002ic seems a less likely explanation than muting effects; other iron-peak features in SN 2005gj are just as strong as in SN 2002ic. Aside from this feature, most of the observed features are generally reproduced. Roughly 22% and 25% of the SDSS *i*-band flux on these two days are accounted for by the spectral template, irrespective of any adjustment to the template color. This discrepancy with the light curve analysis indicates that the template light curve may need to be brighter at this phase than the simple scaling to  $M_B^{peak} = -19.86$  allows.

The implied SN Ia fluxes from the spectral decompositions are indicated in Figure 3. To align the template with the implied SN Ia fraction, the template would need to be 0.12 mag brighter, and either stretched by a factor of 1.32 or shifted by 16 days (or a combination thereof).

Note that as an experiment we also fit the two later-time spectra allowing the phase to float, and find that somewhat better decompositions result from rest-frame phases around 53 days after explosion. The CSM and template are better able to reproduce the emission hump at 5500 Å, but the notch still persists. This difference is more likely to reflect an insufficiency of the spectral decomposition than a slower (or delayed) evolution of the underlying SN Ia. We note that the SDSS *i*-band flux contribution is around 22% at both epochs.

Now we consider the velocity structure, luminosities, and line strength ratios of the H and He emission lines observed. As a starting point, each line was decomposed into a broad and narrow component using two Gaussians. The SN 1991T-like template, multiplied by a linear function, was included in the fit to account for the broad (FWHM  $\sim$ 13000 km s $^{-1}$ ) variations in the background. Where our spectra departs too strongly from the template, as for the H $\beta$  feature, the background was instead accounted for by a second order polynomial.

The results for the line widths and absolute luminosities derived from these two-component Gaussian fits are tabulated in Table 4 and the fits themselves are shown in Figure 8 and 9. The narrow and broad H $\alpha$  features remain constant in flux and width from day 11 to day 71. Both flux variations are less than  $\pm 20\%$  and their velocity variation is on the order of  $\pm 13\%$ . Further, the broad H $\beta$  line width stays constant from day 71 to day 133, suggesting that the widths of the H lines do not evolve over a period of over 4 months. Note that H $\alpha$  from SN 2005gj is much stronger than that from the host.

As noted earlier, the H $\alpha$  feature in the day 71 spectrum and the H $\gamma$ , H $\beta$  and He I  $\lambda$  5876 features in the day 133 spectrum exhibit obvious P Cygni profiles. This morphology rules out an underlying H II region as an explanation for the narrow emission component. We include a P Cygni profile in our fits using a photosphere at  $v_{phot}$  surrounded by a medium with H $\alpha$  optical depth at the photosphere of  $\tau_0$ , exponentially decreasing as  $\exp((v - v_{phot})/v_e)$ . The third free parameter is the density e-folding velocity ( $v_e$ ). The results of these fits are given in Table 5 and the fits are shown in Figures 8 and 9. Note that there is strong covariance between the terms in the P Cygni profile model, and that the spectral resolution places a lower limit on the measurable value of  $v_{phot}$ . Based on our high-resolution fit, we take  $v_{wind} \sim v_{phot} \sim 60$  km s $^{-1}$  as characteristic of the radial velocity of the precursor wind.

Next, we analyze the inverted P Cygni [O III]  $\lambda$ 5007 profile seen in the LRIS spectrum, shown in Figure 4. On day 71, the profile has a net flux of zero, with a flux of  $\sim 7 \times 10^{-17}$  erg cm $^{-2}$  s $^{-1}$  and equivalent width of 0.28 Å measured in both the emission and absorption components. The blue and red components are centered at  $-100$  km s $^{-1}$  and  $+450$  km s $^{-1}$  relative to rest frame, respectively.<sup>5</sup> By day 133, the emission has increased

---

<sup>5</sup>Due to slit effects and instrument flexure, absolute velocities may be uncertain by  $\pm 100$  km s $^{-1}$ . However,

in flux to  $\sim 1.2 \times 10^{-16}$  erg cm $^{-2}$  s $^{-1}$  while the integrated flux deficit in the absorption has decreased to  $\sim 5 \times 10^{-17}$  erg cm $^{-2}$  s $^{-1}$  with an EW  $\sim 0.34$  Å. The emission peak is shifted slightly, to  $-50$  km s $^{-1}$ , while the location of the absorption remains unchanged. The two components have intrinsic widths much less than our 245 km s $^{-1}$  spectral resolution. This feature is discussed further in §5.1.

#### 4. Host Galaxy Properties

The host galaxy of SN 2005gj is barely detectable in our discovery images, however, it is detected in SDSS DR4 (Adelman-McCarthy et al. 2006), as shown in Figure 11, and in the GALEX DR1<sup>6</sup>. The galaxy is elongated, with an ellipticity of  $\sim 0.6$ , and lacks a strong central concentration. The bulk of the galaxy (including the location of SN 2005gj) is very blue (de-reddened  $g-r = +0.18 \pm 0.10$ ,  $r-i = -0.02 \pm 0.13$ ) but the northern tip is extremely red according to the SDSS  $i$  images. Weak H $\alpha$  emission at the redshift of SN 2005gj is present at the location of this northern component in our Keck spectrum. We have compiled the SN 2005gj host photometry in Table 6. Using our measured heliocentric redshift of  $z = 0.0616$ , the absolute magnitude of the host is  $M_B = -17.4$  or  $-16.9$ , depending on whether or not the northern red component is included. The luminosity-metallicity relation for low-luminosity galaxies, recently updated by van Zee, Skillman & Haynes (2006), then suggests a host metallicity in the range  $\log(\text{O/H}) + 12 = 8.2 - 8.3$ .

The GALEX NUV detection and the blue SDSS colors strongly suggest that the light of a recent starburst dominates the blue host component where SN 2005gj appears. Thus, the age of the SN 2005gj progenitor system can most likely be constrained by determining the age of the starburst. In order to constrain the age of the starburst, we have fit the GALEX NUV and SDSS  $ugriz$  photometry to reddened starburst spectra from Leitherer et al. (1999). We chose the grid of instantaneous burst models for a metallicity of  $Z = 0.008$  (supported by the low host luminosity and spectral analysis, below). The Cardelli et al. (1989) extinction law was used to account for Galactic extinction. In order to model the northern red component, we selected a similarly red galaxy, seen in the lower left region of Figure 11 and listed in Table 6, to form a red-component photometric template. A joint fit for the amplitudes of the red and age-dependent starburst templates yields a burst age of  $200 \pm 70$  Myr. The fit has  $\chi^2 = 1.05$  for 3 degrees of freedom, indicating a match slightly better than the quoted photometry errors would predict. The photometry, model

---

relative velocities are more certain, and are therefore quoted to the nearest 50 km s $^{-1}$ .

<sup>6</sup><http://galexgi.gsfc.nasa.gov/targets/DR1/>

components, and resulting fit are shown in Figure 12. This age estimate is sensitive to the assumed amount of Galactic extinction, but can reach no higher than 380 Myr for the case of no Galactic extinction. To our knowledge, this is the strongest constraint ever obtained on the age of a Type Ia supernova progenitor.

Our LRIS spectrum of the region of the host to the south of SN 2005gj shows strong  $\text{H}\alpha$  with  $\text{EW}(\text{H}\alpha) = 35 \text{ \AA}$ , indicative of modest on-going star formation. Another striking feature of the host spectrum is the absence of  $[\text{N II}] \lambda 6584$ ; this is an indicator that the host galaxy metallicity is low (Denicoló et al. 2002). However,  $[\text{S II}] \lambda 6717$  and  $[\text{S II}] \lambda 6730$  are clearly visible. In order to set a better limit on  $[\text{N II}] \lambda 6584$ , we simultaneously fit the restframe 6500–6758  $\text{\AA}$  spectral region, with Gaussian profiles for the emission lines, a linear continuum, plus a scaled version of the SN 2005gj spectrum in order to account for contamination from wings of the PSF of the much brighter SN. The emission lines included in the modeling were  $\text{H}\alpha$ ,  $[\text{N II}] \lambda 6548$ ,  $[\text{N II}] \lambda 6584$ ,  $[\text{S II}] \lambda 6717$ , and  $[\text{S II}] \lambda 6730$ , with  $[\text{N II}] \lambda 6548$  set equal to 0.3 of  $[\text{N II}] \lambda 6584$ . A few pixels badly affected by night sky lines were not included in the fit, but these do not affect any of the regions containing host emission lines. As the flux uncertainty in the remaining spectral region is dominated by the featureless night sky, we assigned uniform weights to each pixel. The weights were set to the inverse variance of the sky, as measured directly from the spectrum. As the wavelength coverage of the fit is very small, no effort was made to account for extinction by dust in this region of the host galaxy.

Our best fit matched the data within the assigned uncertainties. Approximately equal amounts of the continuum were allocated to the scaled spectrum of SN 2005gj and the linear continuum component. Thus, our estimate of  $\text{EW}(\text{H}\alpha)$  given above suffers from pollution by SN 2005gj, both in the  $\text{H}\alpha$  line and in the continuum. Our fit, which accounts for contamination from SN 2005gj, gives  $\text{EW}(\text{H}\alpha) = 44 \text{ \AA}$ .  $[\text{N II}] \lambda 6584$  is not detected; we are able to set a 95% upper limit of  $\log([\text{N II}]/\text{H}\alpha) < -1.24$ . As  $[\text{N II}] \lambda 6584$  can also be suppressed if the ionization parameter is high (see Figure 7 of Kewley & Dopita (2002)), we also examined the  $\text{N II}/\text{S II}$  ratio, which becomes an indicator of the ionization parameter at low metallicities (see Figure 4 of Kewley & Dopita (2002)). We find a 95% confidence upper limit of  $\log([\text{N II}]/[\text{S II}]) < -0.61$ ; this indicates a very low ionization parameter, or possibly an anomalously low abundance of N relative to S. N/S is found to have relatively modest scatter among low-metallicity galaxies (van Zee & Haynes 2006), so it is much more likely that the ionization parameter is low in this case. For low values of the ionization parameter, Kewley & Dopita (2002) show that  $\text{N II}/\text{H}\alpha$  is not very dependent on the ionization parameter. Therefore, we can use our upper limit on  $\log([\text{N II}]/\text{H}\alpha)$  to set a  $2\sigma$  upper limit on the metallicity of  $\log(\text{O/H}) + 12 < 8.2$ . This is consistent with the value expected based on the  $B$ -band luminosity of the host galaxy, derived above, especially when the  $\pm 0.2$  dex scatter in

the luminosity-metallicity relation is included. Using the solar O abundance determined by Allende Prieto et al. (2001), we find that the host of SN 2005gj has  $(Z/Z_{\odot}) < 0.3$ . Deeper observations once SN 2005gj fades away will be needed in order to determine a more accurate abundance.

Finally, it is worth examining the implications of our Galactic and host Na I D measurements. The relation between Na I D and  $E(B-V)$  for stars in the Galaxy exhibits considerable scatter (Herbig 1993; Sembach et al. 1993; Munari & Zwitter 1997). Munari & Zwitter (1997) make the distinction between systems showing Na I D at a single velocity and those with multiple velocity components; this can affect whether the line strengths arise from a single stronger component that may saturate, or from the linear superposition of many weaker — potentially unsaturated — lines. Within our resolution we detect only single components for both Galactic and host extinction. Therefore, we may apply the fit given for Na I D<sub>1</sub> in Table 2 of Munari & Zwitter (1997) to estimate  $E(B-V) \sim 0.2$  from the Galaxy and  $E(B-V) \sim 0.05$  from the host. An alternative prescription based on a mixture of supernova types (Barbon et al. 1990) is clearly non-physical — being linear up to column densities where Na I D must be highly saturated. This may be due to issues with  $E(B-V)$  derived from the colors of highly-extincted supernovae (Wang 2005). Given the dispersion in the relation between Na I D and extinction, we consider the agreement between the Schlegel et al. (1998) and Na I D estimates for Galactic extinction to be reasonable. Based on the weakness of the host (or CSM) Na I D, we consider SN 2005gj to have negligible extinction from its host.

## 5. Discussion

A complete description of the geometry, hydrodynamics, and radiative structure of the CSM surrounding SN 2005gj requires detailed modeling that is beyond the scope of this paper. However, our observations serve as important constraints that any successful model of SN 2005gj must satisfy. More generally, these observations can serve as tests for more generic models designed to account for the apparent variation in the subclass of CSM-interacting SNe.

Here, we summarize our observations and then discuss them in terms of a few crude, but standard, approximations. The light curve of SN 2005gj rose more quickly and to a higher peak luminosity than did SN 2002ic, and declined much more slowly. The earliest spectrum consists of a pseudo-blackbody continuum punctuated by narrow H $\alpha$  emission. Spectra obtained two months after outburst are similar to those of SN 2002ic at the same phase, like those of a “diluted” SN 1991T-like event. These later spectra also include narrow and broad in H $\alpha$ , H $\beta$ , H $\gamma$ , He I  $\lambda 5876$ , and He I  $\lambda 7065$ , with all but He I  $\lambda 7065$  displaying

P Cygni profiles. Blue-shifted higher-level Balmer lines in absorption, each possessing a “shelf” feature to the blue, are observed. The widths of the broad H $\alpha$  and H $\beta$  components do not change with time, the narrow H $\alpha$  luminosity is also fixed, and the observed Balmer decrement is large. Further, we observe a — to our knowledge unique — inverted P Cygni [O III]  $\lambda$ 5007 line.

### 5.1. CSM Density, Mass, Size and Geometry

The early brightness of the light curve relative to that of a SN Ia, the blackbody nature of the spectrum on day 11, and the agreement with the Chugai & Yungelson (2004b) model light curve indicate that SN 2005gj began to interact with its CSM within 7 days of explosion. This time scale and a reasonable estimate for the outer SN ejecta velocity set an upper limit on the inner radius of the CSM. Ejecta velocity at the photosphere of a typical SN Ia 7 days after explosion is 23,000 km s $^{-1}$ , later dropping to 6,000 km s $^{-1}$  (see Figures 10 and 11 of Garavini et al. 2005, and references therein), so we adopt an outer ejecta velocity of  $v_{SN} = 25,000$  km s $^{-1}$  and infer a maximum inner CSM radius of  $R_i^{max} < 1.5 \times 10^{15}$  ( $v_{SN}/25,000$  km s $^{-1}$ ) cm.

While our earliest spectrum allows SN Ia radiation to be present, the overall spectral shape is reasonably accounted for by a blackbody. By scaling an undiluted  $T = 13,000$  K blackbody to our day 11 spectrum we arrive at a bolometric luminosity of  $1.7 \times 10^{44}$  erg s $^{-1}$  at this phase, corresponding to a radius of  $R_{BB} \sim 2.9 \times 10^{15}$  cm. The velocity needed for the SN ejecta to reach this radius in 11 days is  $\sim 30,000$  km s $^{-1}$ . If the explosion date is moved 2 days earlier — in agreement with the Chugai & Yungelson (2004b) light curve fit in the *i*-band — the required ejecta velocity decreases to 25,000 km s $^{-1}$ , in agreement with expectations. This appears to confirm the basic picture that the continuum emission arises from the ejecta/CSM interface. Of course, a spherically symmetric (optically thick) blackbody interaction region is at odds with the detection of the SN Ia component at day 11. It seems that an opening in the interaction region is required for the SN Ia to be seen.

The persistence of strong emission from He I and hydrogen Balmer lines through day 133 may be used to constrain the minimum outer CSM radius. The presence of narrow H $\alpha$  emission and lack of broad H $\alpha$  absorption indicate that the broad hydrogen emission is powered by the shock rather than radioactive decay (Chugai 1991, Table 3). It has become standard to identify the broad emission component with a cooling shock front at the interface between the SN ejecta and CSM. We associate the broad features with the forward shock moving through the hydrogen-rich CSM rather than with the reverse shock propagating into the hydrogen-deficient SN ejecta. Based on the measured velocity widths of the broad

component in Table 4, we take  $v_s = 2,500 \text{ km s}^{-1}$  as representative of the shock velocity (but see discussion below). This is substantially lower than the shock velocity of  $11,000 \text{ km s}^{-1}$  derived by Wang et al. (2004) for SN 2002ic one year after explosion, but in line with the  $2,900 \text{ km s}^{-1}$  inferred by Kotak et al. (2004). Hence, we estimate a minimum outer radius of  $R_o^{\min} > 2.8 \times 10^{15} (v_s/2,500 \text{ km s}^{-1}) \text{ cm}$ .

Note also that the width of the narrow component is much greater than any plausible thermal velocity. These considerations and the presence of a P Cygni profile suggest that the narrow component is associated with unshocked CSM photoionized by the shock. In this case, the broadening could be due to radial expansion of the unshocked material. As the emission may arise from a precursor wind, we denote this velocity as  $v_w$ , and use  $v_w = 60 \text{ km s}^{-1}$  based on the velocity of the P Cygni profile. It is possible that the observed value of  $v_w$  is higher than the historical value of a precursor wind if the pre-shock region is accelerated due to photoionization heating (Chevalier 1997). For a constant  $v_w$ , the derived inner and outer CSM radii imply an outflow beginning at least 15 years ago, and ending less than 8 years prior to explosion.

The observed line strengths may also offer clues to the properties of the CSM. SN 2005gj exhibits a large Balmer decrement —  $\text{H}\alpha/\text{H}\beta \sim 6$  on day 71. If this were due to dust, as is normally assumed when the Balmer decrement departs from case B recombination,  $E(B-V) \sim 0.7$  would be required. This would be at odds with our failure to detect strong Na I D absorption due to the host galaxy. This much dust would require 7 times greater optical luminosity, and in view of the amount of SN light required by our spectral decompositions, the SN Ia required would be unphysical. Moreover, for so much dust there would be very poor agreement between the blackbody radius and the SN ejecta radius at day 11.

Instead, it is more likely that the H level populations are not in case B. The Balmer decrement can be greatly enhanced at high density when the optical depth in the  $\text{H}\alpha$  line is high. Drake & Ulrich (1980) demonstrate this effect for a static slab of H, and attribute it to a combination of Balmer self-absorption (i.e., in which resonant trapping leads to  $\text{H}\beta \rightarrow \text{H}\alpha + \text{P}\alpha$ ) and collisional excitation (also see Xu et al. 1992). The SN-CSM interaction models of Chevalier & Fransson (1994) show this effect, giving  $\text{H}\alpha/\text{H}\beta \sim 7$  after 1 year. Further support for a high-density region comes from the presence of strong He I  $\lambda 7065$  and the lack of evidence for He I  $\lambda 4471$  or  $\lambda 6678$  at day 71. The calculations by Almog & Netzer (1989) suggest that a minimum electron density of  $n_e \sim 10^{10} \text{ cm}^{-3}$  is required to produce such He I line ratios. Clearly, the SN 2005gj line ratios offer a number of interesting clues concerning the nature of the CSM.

As noted in §3.2, a double Gaussian plus P Cygni profile provides an excellent fit to the  $\text{H}\alpha$  and  $\text{H}\beta$  lines. The fits to He I  $\lambda 5876$  and He I  $\lambda 7065$  prefer a flatter, red-shifted

broad component. The question arises as to whether or not these line profiles are consistent with a broad component from a shock front and a narrow component in a photoionized outer region. Fransson (1984) has calculated expected line profiles for emission in SN–CSM shocks. The shapes can be quite complex depending on whether pure scattering dominates over collisional effects, but generally have a roughly parabolic shape or a relatively flat-topped shape. Another case of interest would be that of a shock propagating through a disc, which should give a two-horned profile. None of the example situations give the symmetric Gaussians that we see for the Balmer lines. Indeed, one of the puzzles here is why the broad component would be symmetric at all given that the redshifted portion of the CSM interaction should be occulted by the SN Ia or the optically-thick foreground CSM. On the other hand, the broad components of the He I lines are weak, and probably asymmetric and flat-topped. Therefore, it is unclear how much Balmer emission is co-spatial with the He I lines.

However, Thomson scattering of the lines also must be considered (Chugai 2001; Wang et al. 2004). A simple Monte Carlo simulation shows that for modest optical depth Thomson scattering produces a line profile consisting of a narrow core from unscattered photons and broad wings due to the scattered photons. The width of the broad component and the ratio of the broad and narrow Thomson-scattering components depend on the electron velocity,  $v_e$ , and the scattering optical depth,  $\tau_e$ . As most of the difference between a Thomson-scattering line profile and a simple double-Gaussian occurs in the wings, the undulating SN component makes it difficult to discriminate between these two cases. For a 13,000 K blackbody,  $v_e \sim 760 \text{ km s}^{-1}$ , in rough agreement with the width of the broad component of H $\alpha$ . Our fit to H $\alpha$  using Monte Carlo calculations gives  $\tau_e \sim 1.9$ . An electron density of  $n_e \sim 10^{10} \text{ cm}^{-3}$  and a length scale of order  $l \sim 2 \times 10^{14} \text{ cm}$  gives an Thomson scattering optical depth that agrees with these estimates. This shows that Thomson scattering alone could account for the observed broad hydrogen features for parameters consistent with a shock.

A Thomson-scattering origin for the line widths suggests that both the broad and narrow components of the H emission lines could arise from a single, dense region. This could help to explain why the Balmer decrement is large for the narrow component as well as for the broad component; H $\alpha$ /H $\beta$  for the narrow components would be expected to have close to the case B ratio if they arise, e.g., from photoionization of a protoplanetary nebula. A single origin would also explain why the ratio of the narrow and broad components is not changing appreciably with time. Here the FWHM of the emission lines would no longer be related to  $v_s$ . In this picture there is still material traveling at  $v_w$  in front of the shock, since blue-shifted, P Cygni-like absorption is seen, but a low-density photoionized region from a precursor wind would not be required.

Emission from  $H\alpha$  will be heavily weighted towards high density regions. Assuming regions of roughly constant density, possibly having a filling factor less than unity, we may write the  $H\alpha$  luminosity as:

$$L_{H\alpha} = h\nu_{H\alpha}\alpha_{eff}n_eM/(1.4m_H) \quad (2)$$

where  $M$  is the mass in the shock region and  $\alpha_{eff}$  is the effective H recombination coefficient. Here we assume that the emitting region is 90% H and 10% He by number, and that  $He^+$  and  $He^{++}$  are both present. Wang et al. (2004) took  $\alpha_{eff} = \alpha_B$ , the case B recombination coefficient. However, Chugai (1990) advocates  $\alpha_{eff} = \alpha_C$ , the case C recombination coefficient, when the Balmer optical depth is large, as is the case for the SN 2005gj CSM. Taking  $n_e \sim 10^{10} \text{ cm}^{-3}$  we find that  $M \sim 1.6 \times 10^{-2} (10^{10} \text{ cm}^{-3}/n_e) M_\odot$  is required to explain the observed  $H\alpha$  luminosity. Note that this mass estimate applies only to the mass in the emitting region.

The measured  $L_{H\alpha}$  and inferred Thomson optical depth can be used to set more direct constraints on the dimensions of the emitting region. For example, for  $n_e \sim 10^{10} \text{ cm}^{-3}$  and a radius  $R \sim 2 \times 10^{15} \text{ cm}$ ,  $1.6 \times 10^{-2} M_\odot$  would be contained in a spherical shell with  $\Delta R \sim 3 \times 10^{13} \text{ cm}$ . Such a shell would not be optically thick due to electron scattering and is therefore inconsistent with our measurements. If instead  $n_e \sim 10^{9.0} \text{ cm}^{-3}$ , then the  $H\alpha$ -emitting gas would be  $0.16 M_\odot$  and the shell radius would be  $\Delta R \sim 3 \times 10^{15} \text{ cm}$  and the emitting region would be optically thick to Thomson scattering. Alternatively, as the visibility of the SN requires the presence of an opening in the shock front, we can imagine the emitting region as a working its way through a circumstellar disk. If the emitting region were at a radius  $R \sim 2 \times 10^{15} \text{ cm}$  with mass  $0.016 M_\odot$  the emitting region would have characteristics dimensions of  $\sqrt{l\Delta R} \sim 3 \times 10^{14} \text{ cm}$ , where  $l$  is the thickness. This region would be optically thick to Thomson scattering and this configuration would allow the SN Ia to be easily seen.

More generally, we may combine these basic ingredients to give the value of  $n_e$  that will produce the correct Thomson optical depth and  $H\alpha$  luminosity from a region with characteristic size  $l$ :

$$\bar{n}_e = 0.9 h\nu_{H\alpha}\alpha_{eff}(\tau_e/\sigma_T)^3 L_{H\alpha}^{-1} \quad (3)$$

We find  $\bar{n}_e \sim 1.5 \times 10^8 \text{ cm}^{-3}$  and  $l \sim 2 \times 10^{16} \text{ cm}$ . The total mass in the emitting region would then be  $\sim 0.9 M_\odot$ . This analysis disagrees with our density estimate from the H and He line ratios and the sizes inferred from our SN ejecta speed or blackbody luminosity calculations.

However, if the emitting mass is in the form of  $N_{cld}$  equal clouds, the value of  $\bar{n}_e$  increases in proportion to  $N_{cld}$ ,  $l$  decreases proportionately in order to maintain the electron scattering optical depth for each cloud, and the total mass over all clouds decreases as  $N_{cld}$ . To reach

$n_e \sim 10^{10} \text{ cm}^{-3}$  requires  $\sim 100$  clouds. Such clouds could be similar to fingers from Rayleigh-Taylor instability that produce a corrugated SN-CSM interface in the Chugai et al. (2004c) model for SN 2002ic. Motion of the clouds could contribute to the Gaussian shape of Balmer line profiles, possibly decreasing the electron-scattering optical depth we have inferred.

While electron scattering is able to explain the line profiles we observe, it is worthwhile considering the possibility that the electron scattering optical depth is low. In this case the broad component would be due to the kinematics of the shock. In the thin-shell approximation (Chevalier 1982),  $v_s$  evolves as  $t^{(s-3)/(n-s)}$ , where  $n$  is the power-law index of the density profile of the outer SN ejecta and  $s$  is the power-law index of the CSM material. While SN Ia outer density profiles are not thought to follow a power law,  $n \sim 7$  is often taken as an adequate approximation for application of the self-similar solution of the thin-shell approximation. The constant CSM density,  $s \sim 0$ , profile inferred from the lightcurve then gives  $v_s \propto t^{-3/7}$ . We have measured the Balmer line widths spanning a factor of 10 in time and do not detect any significant change in those widths. The only ways to maintain a constant  $v_s$  are to have  $s \sim 3$  – at odds with the lightcurve – or to have an unphysically steep,  $n \rightarrow \infty$ , outer density profile for the SN ejecta. Thus there is an apparent inconsistency with the classic shock model explanation for the broad component

Further aggravating this inconsistency is the constancy of the Balmer emission. In the shocked region itself, the  $\text{H}\alpha$  luminosity is proportional to the time rate of dissipation of kinetic energy at the shock front,

$$L_{H\alpha}^{\text{Broad}} \sim 1/2 \dot{M}_{CSM} v_s^2$$

where  $\dot{M}_{CSM}$  is the rate at which the CSM is swept up by the shock (Chugai 1991; Salamanca et al. 1998). Therefore the stability of  $L_{H\alpha}^{\text{Broad}}$  requires a very fine tuning between  $\dot{M}_{CSM}$  and  $v_s$ . This is true for any shock, whether or not the broad component is due to electron scattering. In our discussion of electron scattering we considered the case of a large population of clouds. Here, the shock would interact with different clouds at different times, substantially smoothing the emission-weighted  $v_s$  and  $L_{H\alpha}$ .

While determining the exact shape, hydrodynamic state and radiative structure of the CSM would require detailed modeling beyond the scope of this paper, our observations combined with some rough approximations have allowed us to infer that the CSM has a high density and that the optically thick emitting region cannot significantly cover the SN Ia. A high density is also consistent with the absence of detectable X-ray emission (Immler et al. 2005), although the large X-ray opacity of the SN Ia envelope could be equally important (Chugai et al. 2004c). Likewise, the null detection in the radio (Soderberg & Frail 2005) may be due to absorption by thermal electrons in the dense CSM. Line absorption from a circumstellar wind is detected extending out to our last date of observation. The good

agreement of the lightcurve with a flat density profile suggests that the current interaction is not with a classical  $\rho \sim r^{-2}$  wind. Although there is no evidence for delayed CSM interaction, as was seen for SN 2002ic, it is possible that a fast wind from the white dwarf has piled up material where the interaction is now occurring (Chevalier 1997). Alternatively, the mass loss may have tapered off with time, producing a flatter density profile. The mass of the emitting region is quite small if the densities are as high as we have inferred. Unlike the classical case where the narrow Balmer emission arises from the photoionized precursor wind, in our picture we can not use Equation 2 to place a lower limit on the mass in the wind. Therefore, the total CSM mass remains uncertain, and will have to be estimated using a self-consistent radiative hydrodynamic model.

One remaining clue to the nature of the SN-CSM interaction is the inverted P Cygni profile of [O III]  $\lambda 5007$  seen in the Keck spectra on days 71 and 133. The inverted P Cygni profile morphology is extremely interesting, and could indicate that the line forms in a region that is excited from the outside rather than from the SN, and forms in the intershock region. A very high density is required to achieve sufficient optical depth for absorption in the line. The oxygen abundance of high-velocity SN Ia material should be much higher than that found in the CSM (Hatano et al. 1999) and therefore we conclude that the feature is most likely to originate within the SN ejecta.

## 5.2. Progenitor Models

One of the potentially powerful applications of rare events like SN 2005gj is in understanding the progenitor systems of SNe Ia. While the interaction with the CSM provides many clues to the progenitor system, the host galaxy environment adds additional information and helps to place such events in the context of star formation and evolution models. SN 2005gj is a rare example in which observations of the host galaxy place interesting constraints on the likely progenitor age and metallicity. In this section we explore the broader implications of our host-galaxy measurements.

If the progenitor system of SN 2005gj shares the approximately 200 Myr age of the starburst dominating the host galaxy, this places some constraints on the allowed parameters of the progenitor system. A  $3 M_{\odot}$  star – thought to be the minimum mass for forming a Type Ia from a carbon-oxygen white dwarf – will take 400 Myr to complete its He-burning phase according to the evolutionary models of Schaerer et al. (1993) for stars with  $Z/Z_{\odot} = 0.4$ . A  $4 M_{\odot}$  star requires only 190 Myr. Thus, the inferred age of the starburst is quite consistent with the mass range of SN Ia progenitors derived from other stellar evolution calculations (see Umeda, et al. 1999, and references therein). Simulations by Belczynski et al.

(2005) indicate that, for their fiducial model parameter settings, both single-degenerate and double-degenerate channels will just barely have become operative 200 Myr after birth of the progenitor system. Better agreement with a 200 Myr timescale is obtained by decreasing the CE efficiency factor. Broadly speaking, single-degenerate progenitors tend to have timescales that are strongly clumped in the 200 to 800 Myr timescale, while double-degenerate progenitors tend to occur more uniformly over a 100 Myr to 10 Gyr timescale. Thus, the age of the host starburst is consistent with modeled timescale estimates for both single-degenerate and double-degenerate progenitors. On the other hand, if SN 2005gj is associated with the old stellar population in its host galaxy, the Belczynski et al. (2005) models suggest that the double-degenerate scenario would dominate after several Gyr.

The low metallicity derived for the host galaxy may be important in understanding SN 2005gj. The metallicity is likely to have an impact on how quickly the winds from the progenitor or donor star can be swept out of the system via radiation pressure from a hot WD, with low metallicity increasing the likelihood that CSM will be present when the SN Ia eventually explodes. Extreme metallicities may even lead to new channels for thermonuclear SNe. For example, Tsujimoto (2006) argue that metal-free ( $[\text{Fe}/\text{H}] < -5$ ) stars in the range  $3.5M_{\odot} < M < 7M_{\odot}$  could explode as thermonuclear SNe inside a dense unburned hydrogen envelope. This is close to the Type 1.5 scenario where the carbon-oxygen core of a single massive asymptotic giant branch star undergoes a thermonuclear explosion (Hamuy et al. 2003). While we have only an upper limit on the likely metallicity of the progenitor system based on the host galaxy, it seems unlikely that the metallicity is as low as required in this scenario. Zijlstra (2004) has suggested that a low mass loss rate from an AGB star due to low metallicity could allow the carbon-oxygen core to reach the Chandrasekhar limit, leading to a Type 1.5. An example is a star with  $[\text{Fe}/\text{H}] = -1$  and an initial mass of  $6.5 M_{\odot}$ ; such a star would complete its evolution in  $\sim 60$  Myr (Schaller et al. 1992; Schaerer et al. 1993). A progenitor star of such mass is unlikely given our starburst age estimate, but a progenitor of slightly lower mass would be allowed. In the Zijlstra (2004) scenario, this would require  $[\text{Fe}/\text{H}] < -1$ , and would require that the metallicity of the host of SN 2005gj fall significantly below the standard galaxy luminosity-metallicity relation.

More apropos would be the studies such as Kobayashi et al. (1998); Kato & Hachisu (1999) examining the relation between progenitor metallicity and accretion onto a classical carbon-oxygen WD. They find that at low metallicity the deposition rate is too high due to the reduced radiation pressure from the WD on the infalling material; low metallicity systems thus fail to produce Type Ia events. Kobayashi et al. (1998) present the allowed values of donor mass and orbital period for solar and  $0.2 \times$  solar abundance for a main sequence donor and red giant donor. Our age limit from the host starburst precludes their  $1 M_{\odot}$  red giant as a donor, while our upper limit of  $Z/Z_{\odot} < 0.3$  shrinks the allowed mass of the main sequence

donor in their models to  $\sim 2.2 \pm 0.4 M_{\odot}$  (and an orbital period in the range  $0.4 < P < 4$  days; the range of separation between the donor and a white dwarf of  $1.4 M_{\odot}$  placed by these limits is  $2.3 \times 10^{11} \text{ cm} < a < 1.7 \times 10^{12} \text{ cm}$ ).

Other possibilities include the Livio & Riess (2003) model for SN 2002ic, in which the merger of two white dwarfs immediately follows a common envelope (CE) phase. In this model, the merger due to gravitational radiation occurs after a common envelope stage has finished expelling mass from the system. Chugai & Yungelson (2004b, eq. (3)) argue against this scenario in the case of SN 2002ic because the white dwarf and core cannot get close enough to merge via gravitational radiation on a timescale commensurate with the presence of CSM. Getting the white dwarf and core sufficiently close would require removal of energy via the envelope, but the observed CSM velocities are simply too low. This is also the case for SN 2005gj. We infer that mass loss ended at most 8 years prior to explosion, so as with SN 2002ic, the timescale for gravitational wave radiation after the CE phase is very short. Likewise, the velocity required for removal of sufficient energy via the envelope is too low by well over an order of magnitude.

Perhaps more interesting in the case of SN 2005gj is the scenario recently described by Han & Podsiadlowski (2006) in which a delayed dynamical instability operating over a period of  $\sim 10^4$  yrs allows a  $\sim 3 M_{\odot}$  donor star to eject  $\sim 2 M_{\odot}$  of material out of the binary system while a trickle of mass builds up an already massive WD to the point of thermonuclear explosion. While constructed to explain SN 2002ic, this model seems to be consistent with what we have been able to infer from our observations of SN 2005gj. More detailed modeling of SN 2005gj will be needed, however, in order to test the Han & Podsiadlowski (2006) scenario. This model gives in a predicted incidence of CSM-interacting SNe Ia in the range 0.001–0.01, which agrees within the large uncertainties with the 2–4 such systems discovered over the past 10 years in which  $\sim 550$  nearby SNe Ia have been reported. A prediction of the Han & Podsiadlowski (2006) model — which did not arise directly from SN 2002ic — is that the highest incidence of such events will occur 0.1–1 Gyr after the birth of the progenitor system; our age estimate for SN 2005gj falls squarely within this window.

In a cosmological context it is interesting to ask whether a SN Ia like SN 2002ic or SN 2005gj could mistakenly be included among a sample of normal SN Ia used to fit for the cosmological parameters. At high redshift the H $\alpha$  emission feature in our day 11 spectrum would be redshifted out of the typical observing window. Thus, an observer would see the smooth spectrum of a hot blackbody, likely superimposed on the spectrum of a blue host galaxy, and probably classify the event has an early, overluminous SN II. Several examples matching this description are shown in Lidman et al. (2005). At later times, when the

classical SN Ia features are apparent, the diluting affects of the CSM emission could be mistaken for host galaxy light, e.g., from a starburst, resulting in a SN Ia classification (See Lidman et al. 2005; Hook et al. 2005, for descriptions of the standard spectral classification techniques applied at high redshift). A much stronger discriminant is the lightcurve shape. In the case of SN 2005gj, the flat lightcurve would be a clear indicator of a serious problem. However, as can be seen in Wood-Vasey et al. (2004) for the case of SN 2002ic — for which the CSM interaction is weaker and its onset delayed — lightcurve data at least 40 days after maximum light would be needed to detect a problem. Such data usually was not available in the Supernova Cosmology Project or High-Z Supernova Search Team SN Ia cosmology searches of the late 1990’s. More modern rolling searches such as the Supernova Legacy Survey (Astier et al. 2006) and ESSENCE (Krisciunas et al. 2005) contain such data except for SNe Ia discovered late relative to the observing window for a given program field. As the high-redshift SN Ia searches have netted several hundred events to date, events like SN 2005gj and SN 2002ic should have been detected unless their incidence declines strongly with redshift. In fact, the opposite trend is expected, as the type of low-metallicity starburst likely to have spawned SN 2005gj should be more prevalent at high redshift.

SN 2005gj, SN 2002ic, and SN 1997cy all exhibit large CSM interactions and arose in low-luminosity hosts. This underscores the importance of blind searches that are not biased towards bright known hosts for surveys that aim to provide data for understanding SN Ia physics. It also raises questions about the consistency between the currently available nearby SNe sample (taken mostly from targeted galaxy searches) and the distant SNe sample (taken primarily from untargeted searches).

## 6. Conclusions

First classified as Type IIn and then displaying clear Type Ia features, SN 2005gj is the second supernova spectroscopically confirmed to possess Type Ia features combined with a strong CSM interaction. Of these two confirmed events and two suspected such events, SN 2005gj presented the largest observed CSM interaction, and its early behavior raises the question of how many of the early detected SNe IIn might be similar events.

The lightcurve and spectroscopy presented here offer a wealth of information. Much more detailed modeling will help in understanding the nature of progenitor system, and could be a key to understanding important aspects of the formation of Type Ia supernovae. Better statistics from larger unbiased nearby supernova searches will help greatly in understanding the possibly multiple channels that produce SNe Ia.

The authors are grateful to the technical and scientific staffs of the University of Hawaii 2.2-meter telescope, the W. M. Keck Observatory, Palomar Observatory, the QUEST-II collaboration, and HPWREN, for their assistance in obtaining these data. Some of the data presented herein were obtained at the W. M. Keck Observatory, which is operated as a scientific partnership among the California Institute of Technology, the University of California, and the National Aeronautics and Space Administration. The Observatory was made possible by the generous financial support of the W. M. Keck Foundation. We thank K Barbary and K. Dawson for their assistance with the Keck LRIS observations, and S. Ferrell for assistance with photometry of the NEAT images. The authors wish to recognize and acknowledge the very significant cultural role and reverence that the summit of Mauna Kea has always had within the indigenous Hawaiian community. We are most fortunate to have the opportunity to conduct observations from this mountain. This work was supported in part by the Director, Office of Science, Office of High Energy and Nuclear Physics, of the U.S. Department of Energy under Contracts No. DE-FG02-92ER40704, by a grant from the Gordon & Betty Moore Foundation, by National Science Foundation Grant Number AST-0407297, and in France by support from CNRS/IN2P3, CNRS/INSU and PNC. This research used resources of the National Energy Research Scientific Computing Center, which is supported by the Office of Science of the U.S. Department of Energy under Contract No. DE-AC03-76SF00098. We thank them for a generous allocation of storage and computing time. HPWREN is funded by National Science Foundation Grant Number ANI-0087344, and the University of California, San Diego. Funding for the Sloan Digital Sky Survey (SDSS) has been provided by the Alfred P. Sloan Foundation, the Participating Institutions, the National Aeronautics and Space Administration, the National Science Foundation, the U.S. Department of Energy, the Japanese Monbukagakusho, and the Max Planck Society. The SDSS Web site is <http://www.sdss.org/>. GALEX is a NASA Small Explorer, launched in April 2003. We gratefully acknowledge NASA's support for construction, operation, and science analysis for the GALEX mission.

*Facilities:* PO:1.2m (QUEST-II), UH:2.2m (SNIFS), Keck:I (LRIS), GALEX

## REFERENCES

- Adelman-McCarthy, J., Agueros, M.A., Allam, S.S., et al. 2006, ApJS, in press (Data Release 4)
- Aldering, G., et al. 2002, Proc. SPIE, 4836, 61
- Allende Prieto, C., Lambert, D. L., & Asplund, M. 2001, ApJ, 556, L63

- Almog, Y., & Netzer, H. 1989, MNRAS, 238, 57
- Astier, P., *et al.* 2006, A&A, 447, 31
- Bacon, R., *et al.* 1995, A&AS, 113, 347
- Bacon, R., Emsellem, E., Copin, Y., & Monnet, G. 2000, ASP Conf. Ser. 195: Imaging the Universe in Three Dimensions, 195, 173
- Bacon, R., *et al.* 2001, MNRAS, 326, 23
- Barbon, R., Benetti, S., Rosino, L., Cappellaro, E., & Turatto, M. 1990, A&A, 237, 79
- Barentine, J. *et al.*, CBET 247.
- Beland, S., Boulade, O. & Davidge, T. 1988, CFHT Info. Bull. 19, 16
- Belczynski, K., Bulik, T., & Ruiter, A. J. 2005, ApJ, 629, 915
- Berger, E., Soderberg, A. M., & Frail, D. A. 2003, IAU Circ., 8157, 2
- Bertin, E., & Arnouts, S. 1996, A&AS, 117, 393
- Branch, D., Livio, M., Yungelson, L. R., Boffi, F. R., & Baron, E. 1995, PASP, 107, 1019
- Branch, D., Jeffery, D. J., Blaylock, M., & Hatano, K. 2000, PASP, 112, 217
- Cardelli, J. A., Clayton, G. C., & Mathis, J. S. 1989, ApJ, 345, 245
- Chevalier, R. A., 1982, ApJ, 258, 790
- Chevalier, R. A., & Fransson, C. 1994, ApJ, 420, 268
- Chevalier, R. A. 1997, ApJ, 488, 263
- Chugai, N. N. 1990, Soviet Ast., 16, 457
- Chugai, N. N. 1991, MNRAS, 250, 513
- Chugai, N. N. 2001, MNRAS, 326, 1448
- Chugai, N. N., *et al.* 2004a, MNRAS, 352, 1213
- Chugai, N. N. & Yungelson, L. R., 2004b, AstL, 30, 65
- Chugai, N. N., Chevalier, R. A., & Lundqvist, P. 2004c, MNRAS, 355, 627

- Deng, J., et al. 2004, *ApJ*, 605, L37
- Denicoló, G., Terlevich, R., & Terlevich, E. 2002, *MNRAS*, 330, 69
- Drake, S. A., & Ulrich, R. K. 1980, *ApJS*, 42, 351
- Drell, P. S., Loredo, T. J., & Wasserman, I. 2000, *ApJ*, 530, 593
- Ferrara, A., & Tolstoy, E. 2000, *MNRAS*, 313, 291
- Filippenko, A. V., 1982, *PASP*, 94, 715
- Fransson, C. 1984, *A&A*, 132, 115
- Frieman, J. 2005, *IAU Circ.*, 8616, 1
- Garavini, G., et al. 2005, *AJ*, 130, 2278
- Garnavich, P. M., et al. 1998, *ApJ*, 493, L53
- Hamuy, M., Phillips, M. M., Suntzeff, N. B., Maza, J., Gonzalez, L. E., Roth, M., Krisciunas, K., Morrell, N., Green, E. M., Persson, S. E., & McCarthy, P. J. 2003, *Nature*, 424, 651
- Han, Z., & Podsiadlowski, P. 2006, *astro-ph/0602229*
- Hanuschik, R. W. 2003, *A&A*, 407, 1157
- Hatano, K., Branch, D., Fisher, A., Millard, J., & Baron, E. 1999, *ApJS*, 121, 233
- Herbig, G. H. 1993, *ApJ*, 407, 142
- Hook, I. M., et al. 2005, *AJ*, 130, 2788
- Howell, D. A. 2001, *ApJ*, 554, L193
- Iben, I., & Renzini, A. *ARA&A*, 21, 271
- Immler, S., Petre, R., & Brown, P., 2005, *IAU Circ.*, 8633, 2
- Kato, M., & Hachisu, I. 1999, *ApJ*, 513, L41
- Kewley, L. J., & Dopita, M. A. 2002, *ApJS*, 142, 35
- Knop, R. A., et al. 2003, *ApJ*, 598, 102
- Kobayashi, C., Tsujimoto, T., Nomoto, K., Hachisu, I., & Kato, M. 1998, *ApJ*, 503, L155

- Kotak, R., Meikle, W. P. S., Adamson, A., & Leggett, S. K. 2004, MNRAS, 354, L13
- Krisciunas, K., et al. 2005, AJ, 130, 2453
- Kwok, S. 1993, ARA&A, 31, 63
- Lantz, B., et al. 2004, Proc. SPIE, 5249, 146
- Leibundgut, B. 2001, ARA&A, 39, 67
- Leitherer, C., et al. 1999, ApJS, 123, 3
- Lidman, C., et al. 2005, A&A, 430, 843
- Livio, M., & Riess, A. G. 2003, ApJ, 594, L93
- Mazzali, P. A., Danziger, I. J., & Turatto, M. 1995, A&A, 297, 509
- Monet, D., et al. 1996, USNO-A1.0 Catalog (Washington: US Naval Obs.)
- Munari, U., & Zwitter, T. 1997, A&A, 318, 269
- Nugent, P., Kim, A. G., & Perlmutter, S., 2002, PASP, 114, 803
- Oke, J. B., et al. 1995, PASP, 107, 375
- Perlmutter, S., et al. 1998, Nature, 391, 51
- Perlmutter, S., et al. 1999, ApJ, 517, 565
- Phillips, M. M., Lira, P., Suntzeff, N. B., Schommer, R. A., Hamuy, M., & Maza, J., 1999, AJ, 118, 1766
- Prieto, J., Garnavich, P., Depoy, D., Marshall, J., Eastman, J., & Frank, S. 2005, IAU Circ., 8633, 1
- Pinto, P. A., & Eastman, R. G. 2000, ApJ, 530, 757
- Scannapieco, E., & Bildsten, L. 2005, ApJ, 629, L85
- Storey, P. J., & Hummer, D. G. 1995, MNRAS, 272, 41
- Rabinowitz, D. et al. 2003, American Astronomical Society Meeting 203, #38.12
- Riess, A. G., et al. 1998, AJ, 116, 1009
- Riess, A. G., et al. 2004, ApJ, 607, 665

- Riess, A. G., et al. 2005, ApJ, 627, 579
- Saha, A., Sandage, A., Thim, F., Labhardt, L., Tammann, G. A., Christensen, J., Panagia, N., & Macchietto, F. D., 2001, ApJ, 551, 973
- Salamanca, I., Cid-Fernandes, R., Tenorio-Tagle, G., Telles, E., Terlevich, R. J., & Munoz-Tunon, C. 1998, MNRAS, 300, L17
- Schaerer, D., Meynet, G., Maeder, A., & Schaller, G. 1993, A&AS, 98, 523
- Schaller, G., Schaerer, D., Meynet, G., & Maeder, A. 1992, A&AS, 96, 269
- Schlegel, D. J., Finkbeiner, D. P., & Davis, M. 1998, ApJ, 500, 525
- Schlegel, E. M. 1990, MNRAS, 244, 269
- Schwank, M., Schmutz, W., & Nussbaumer, H. 1997, A&A, 319, 166
- Sembach, K. R., Danks, A. C., & Savage, B. D. 1993, A&AS, 100, 107
- Soderberg, A. M. & Frail, D. A., 2005, ATel, 663
- Stockdale, C. J., Sramek, R. A., Weiler, K. W., Van Dyk, S. D., Panagia, N., Hamuy, M., & Berger, E. 2003, IAU Circ., 8157, 3
- Tonry, J. L., et al. 2003, ApJ, 594, 1
- Tripp, R. & Branch, D., 1999, ApJ, 525, 209
- Tsujimoto, T. 2006, astro-ph/0601324
- Uenishi, T., Suzuki, T., Nomoto, K., & Hachisu, I. 2004, Revista Mexicana de Astronomia y Astrofisica Conference Series, 20, 219
- Umeda, H., Nomoto, K., Yamaoka, H., & Wanajo, S. 1999, ApJ, 513, 861
- van Zee, L., & Haynes, M. P. 2006, ApJ, 636, 214
- van Zee, L., Skillman, E., & Haynes, M. P. 2006, ApJ, 637, 269
- Wang, L., Goldhaber, G., Aldering, G., & Perlmutter, S., 2003, ApJ, 590, 944
- Wang, L. 2005, ApJ, 635, 33
- Wang, L., et al. Strovink, M., Conley, A., Goldhaber, G., Kowalski, M., Perlmutter, S., & Siegrist, J., 2005, ApJ submitted, astro-ph/0512370

- Wang, L., Baade, D., Höflich, P., Wheeler, J. C., Kawabata, K., & Nomoto, K. 2004, ApJ, 604, L53
- Wood-Vasey, W. M. 2002, IAU Circ., 8019, 2
- Wood-Vasey, W. M., Wang, L., & Aldering, G. 2004, ApJ, 616, 339
- Xu, Y., McCray, R., Oliva, E., & Randich, S. 1992, ApJ, 386, 181
- Zijlstra, A. A. 2004, MNRAS, 348, L23

Table 1: SDSS *i* Photometric Observations of SN 2005gj.

| Julian Day | Camera   | Filter           | SDSS <i>i</i> Magnitude |
|------------|----------|------------------|-------------------------|
| 2453636.91 | QUEST-II | RG610            | < 20.15                 |
| 2453642.95 | QUEST-II | RG610            | $18.02 \pm 0.06$        |
| 2453647.09 | SNIFS    | Synthesized      | $17.78 \pm 0.10$        |
| 2453647.95 | QUEST-II | RG610            | $17.56 \pm 0.05$        |
| 2453648.91 | QUEST-II | Johnson <i>I</i> | $17.53 \pm 0.04$        |
| 2453651.78 | QUEST-II | Johnson <i>I</i> | $17.29 \pm 0.04$        |
| 2453654.91 | QUEST-II | Gunn <i>i</i>    | $17.34 \pm 0.04$        |
| 2453656.91 | QUEST-II | Gunn <i>i</i>    | $17.18 \pm 0.05$        |
| 2453667.84 | QUEST-II | RG610            | $16.98 \pm 0.06$        |
| 2453670.90 | QUEST-II | RG610            | $16.97 \pm 0.07$        |
| 2453670.90 | QUEST-II | RG610            | $17.00 \pm 0.06$        |
| 2453692.90 | QUEST-II | RG610            | $16.88 \pm 0.09$        |
| 2453692.94 | QUEST-II | RG610            | $17.24^{+0.36}_{-0.27}$ |
| 2453699.96 | SNIFS    | Synthesized      | $17.07 \pm 0.04$        |
| 2453702.70 | QUEST-II | RG610            | $17.03 \pm 0.06$        |
| 2453706.96 | SNIFS    | Synthesized      | $17.12 \pm 0.04$        |
| 2453706.98 | SNIFS    | Synthesized      | $17.07 \pm 0.04$        |

---

Note. — Synthesized photometry is from flux-calibrated SNIFS spectra

Table 2: *V*-band photometry of SN 2005gj.

| Julian Day | Camera   | Filter           | Johnson <i>V</i> Magnitude |
|------------|----------|------------------|----------------------------|
| 2453642.95 | QUEST-II | RG610            | $17.90 \pm 0.09$           |
| 2453647.09 | SNIFS    | Synthesized      | $17.59 \pm 0.15$           |
| 2453647.95 | QUEST-II | RG610            | $17.57 \pm 0.10$           |
| 2453648.91 | QUEST-II | Johnson <i>R</i> | $17.48 \pm 0.04$           |
| 2453651.78 | QUEST-II | Johnson <i>R</i> | $17.34 \pm 0.05$           |
| 2453648.91 | QUEST-II | Johnson <i>B</i> | $17.48 \pm 0.08$           |
| 2453651.78 | QUEST-II | Johnson <i>B</i> | $17.27 \pm 0.08$           |
| 2453654.92 | QUEST-II | Gunn <i>r</i>    | $17.37 \pm 0.04$           |
| 2453656.91 | QUEST-II | Gunn <i>r</i>    | $17.35 \pm 0.04$           |
| 2453667.84 | QUEST-II | RG610            | $17.20 \pm 0.09$           |
| 2453670.90 | QUEST-II | RG610            | $17.22 \pm 0.10$           |
| 2453670.90 | QUEST-II | RG610            | $17.18 \pm 0.10$           |
| 2453699.96 | SNIFS    | Synthesized      | $17.41 \pm 0.15$           |
| 2453702.70 | QUEST-II | RG610            | $17.45 \pm 0.09$           |
| 2453706.96 | SNIFS    | Synthesized      | $17.46 \pm 0.15$           |
| 2453706.98 | SNIFS    | Synthesized      | $17.41 \pm 0.15$           |

Note. — QUEST-II photometry is based upon extrapolations from Johnson *R*, Johnson *B*, Gunn *r*, and RG610 filters, using SNIFS spectra for the color corrections. Synthesized photometry is from flux-calibrated SNIFS spectra.

Table 3. Journal of Spectroscopic Observations of SN 2005gj.

| Julian Day | UTC Date      | Range<br>(Å) | Resolution <sup>a</sup><br>Blue : Red (Å) | Exposure<br>(s) | Airmass | Facility      | Conditions       |
|------------|---------------|--------------|---|-----------------|---------|---------------|------------------|
| 2453647.09 | 2005-10-03.59 | 3501-9994    | 2.6 : 3.5                                 | 1000            | 1.16    | UH88 + SNIFS  | cloudy           |
| 2453699.96 | 2005-11-25.46 | 3501-9994    | 2.6 : 3.5                                 | 1400            | 1.23    | UH88 + SNIFS  | photometric      |
| 2453706.83 | 2005-12-02.33 | 3225-9489    | 12 : 8.2                                  | 900             | 1.08    | Keck I + LRIS | non-photometric  |
| 2453706.96 | 2005-12-02.46 | 3501-9994    | 2.6 : 3.5                                 | 1400            | 1.31    | UH88 + SNIFS  | near-photometric |
| 2453706.98 | 2005-12-02.48 | 3501-9994    | 2.6 : 3.5                                 | 1400            | 1.46    | UH88 + SNIFS  | near-photometric |
| 2453768.23 | 2006-02-02.23 | 3500-6755    | 6.5 : 1.8                                 | 900             | 1.11    | Keck I + LRIS | photometric      |

<sup>a</sup> LRIS resolution is seeing dependent

Table 4. Emission line fits using two Gaussians plus continuum.

| Source | Line       | Day | Broad Component    |                 |  | Narrow Component     |                   |  | Luminosity<br>(erg/s) |                      |
|--------|------------|-----|--------------------|-----------------|--|----------------------|-------------------|--|-----------------------|----------------------|
|        |            |     | $\lambda_0$<br>(Å) | $\sigma$<br>(Å) | FWHM <sup>a</sup><br>(km s <sup>-1</sup> ) | $\lambda_0$<br>(Å)   | $\sigma^a$<br>(Å) | FWHM <sup>b</sup><br>(km s <sup>-1</sup> ) |                       |                      |
| SNIFS  | H $\alpha$ | 11  | 6563.9             | 16.3            | 1670                                       | 6.7 $\times 10^{40}$ | 6563.3            | 3.5  | unresolved            | $2.3 \times 10^{40}$ |
| SNIFS  | H $\alpha$ | 64  | 6564.8             | 20.7            | 2140                                       | 7.7 $\times 10^{40}$ | 6564.4            | 4.1  | unresolved            | $3.6 \times 10^{40}$ |
| SNIFS  | H $\alpha$ | 71  | 6564.6             | 21.3            | 2210                                       | 8.4 $\times 10^{40}$ | 6564.5            | 4.0  | unresolved            | $3.2 \times 10^{40}$ |
| LRIS   | H $\alpha$ | 71  | 6564.5             | 18.1            | 1870                                       | 5.4 $\times 10^{40}$ | 6563.6            | 2.2  | unresolved            | $2.3 \times 10^{40}$ |
| LRIS   | H $\beta$  | 71  | 4862.1             | 14.0            | 1710                                       | 1.1 $\times 10^{40}$ | 4863.4            | 3.6  | unresolved            | $6.9 \times 10^{39}$ |
| LRIS   | H $\beta$  | 133 | 4859.9             | 12.7            | 1780                                       | 1.6 $\times 10^{40}$ | 4862.4            | 1.4  | unresolved            | $3.7 \times 10^{39}$ |
| LRIS   | He I       | 133 | 5876.8             | 20.7            | 1740                                       | 1.2 $\times 10^{40}$ | 5876.4            | 0.8  | 60                    | $1.0 \times 10^{39}$ |

<sup>a</sup>Covariance between the width of the narrow component and the broad component, or with the P Cygni line, can lead to a best-fit width that is slightly wider or narrower than the spectrograph resolution.

<sup>b</sup>FWHM is reported only when width due to spectrograph resolution can be meaningfully removed.

Table 5. Emission line fits including P Cygni profile

| Source | Line       | Day | Broad Component    |                 |  | Narrow Component   |                 |  | P Cygni Component                     |                                     |                                  |
|--------|------------|-----|--------------------|-----------------|--|--------------------|-----------------|--|---------------------------------------|-------------------------------------|----------------------------------|
|        |            |     | $\lambda_0$<br>(Å) | $\sigma$<br>(Å) | FWHM <sup>a</sup><br>(km s <sup>-1</sup> ) | $\lambda_0$<br>(Å) | $\sigma$<br>(Å) | FWHM <sup>a</sup><br>(km s <sup>-1</sup> ) | $v_{phot}^b$<br>(km s <sup>-1</sup> ) | $\tau_0^c$<br>(km s <sup>-1</sup> ) | $v_e^d$<br>(km s <sup>-1</sup> ) |
| LRIS   | H $\alpha$ | 71  | 6562.1             | 19.5            | 2020                                       | 6563.7             | 2.3             | unresolved                                 | 282                                   | 5.9                                 | 51                               |
| LRIS   | H $\beta$  | 133 | 4861.6             | 12.4            | 1740                                       | 4862.4             | 4.5             | unresolved                                 | 251                                   | 189                                 | 6                                |
| LRIS   | He I       | 133 | 5880.2             | 27.6            | 3240                                       | 5876.1             | 1.0             | unresolved                                 | 60                                    | 0.3                                 | 50                               |

<sup>a</sup>FWHM is reported only when width due to spectrograph resolution can be meaningfully removed.

<sup>b</sup>Photospheric velocity

<sup>c</sup>Optical depth at the photosphere

<sup>d</sup>e-folding velocity

Table 6: Dereddened magnitudes for the SN 2005gj host galaxy.

| Source | Band | SDSS<br>Parent   | SDSS<br>Child A  | SDSS<br>Child B  | SDSS<br>Red Template |
|--------|------|------------------|------------------|------------------|----------------------|
| GALEX  | FUV  | ...              | ...              | ...              | ...                  |
| GALEX  | NUV  | $20.74 \pm 0.26$ | ...              | ...              | ...                  |
| SDSS   | u    | $20.27 \pm 0.30$ | $20.76 \pm 0.38$ | $22.39 \pm 1.43$ | +0.12                |
| SDSS   | g    | $19.60 \pm 0.05$ | $20.13 \pm 0.06$ | $21.21 \pm 0.14$ | +0.00                |
| SDSS   | r    | $19.32 \pm 0.06$ | $19.95 \pm 0.08$ | $20.48 \pm 0.10$ | -1.69                |
| SDSS   | i    | $18.91 \pm 0.04$ | $19.97 \pm 0.10$ | $19.69 \pm 0.06$ | -2.80                |
| SDSS   | z    | $18.70 \pm 0.12$ | $19.09 \pm 0.13$ | $19.49 \pm 0.18$ | -3.28                |

Note. — SDSS dereddened magnitudes are given for the two deblended components as well as the SDSS parent object (SN 2005gj resides in the part of the galaxy characterized by component Child A). The last column gives the  $g - m_\lambda$  colors of the galaxy at  $\alpha = 45:18:04.25$ ,  $\delta = -00:33:30.7$  (J2000) used as a template for the red component of the host of SN 2005gj. As this is used as a template, we assign no uncertainty — however doing so would make our  $\chi^2/\text{DOF}$  far too small. The GALEX spatial resolution of  $7''$  means that the host will be seen as a point source, so it cannot be decomposed into components matching the SDSS children. Note that when fitting for the age, we redden the model, rather than unreden the data in order to correctly account for differential extinction across filter bandpasses.

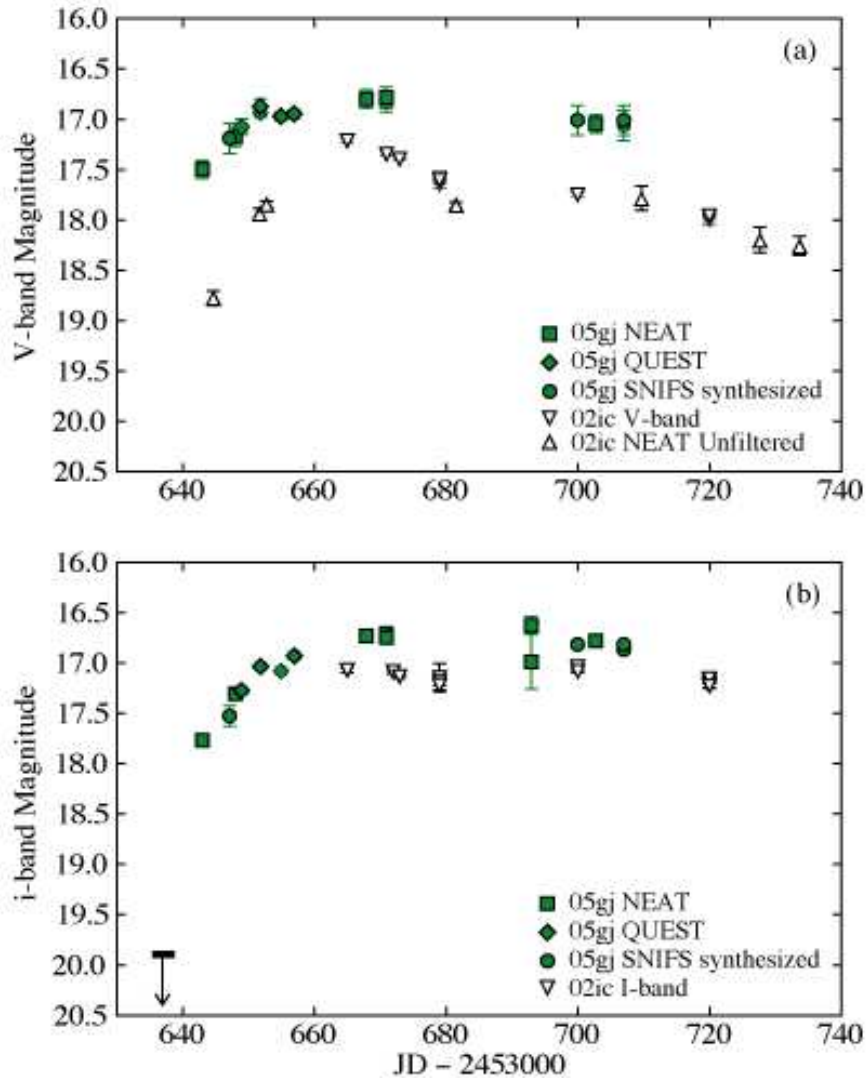


Fig. 1.— Lightcurve of SN 2005gj in  $V$ -band (a) and  $i$ -band (b). SN 2002ic observations are overlaid in  $V$ -band and NEAT unfiltered (a) and  $I$ -band (b). The SN 2005gj  $V$ -band data are extrapolations from other filters based upon the shape of the SNIFS spectra. The time axis of the SN 2002ic data has been shifted to align the estimated explosion dates of 2002 November 5 and 2005 September 22.6 UTC. All datapoints have been extinction corrected, and the SN 2002ic datapoints have been adjusted for the cosmological effects — but not the bandpass shift — due to the small difference in redshift. Wood-Vasey et al. (2004) report that the 2002–2003 NEAT unfiltered photometry is comparable to  $V$ -band photometry to within  $\pm 0.05$  mag.

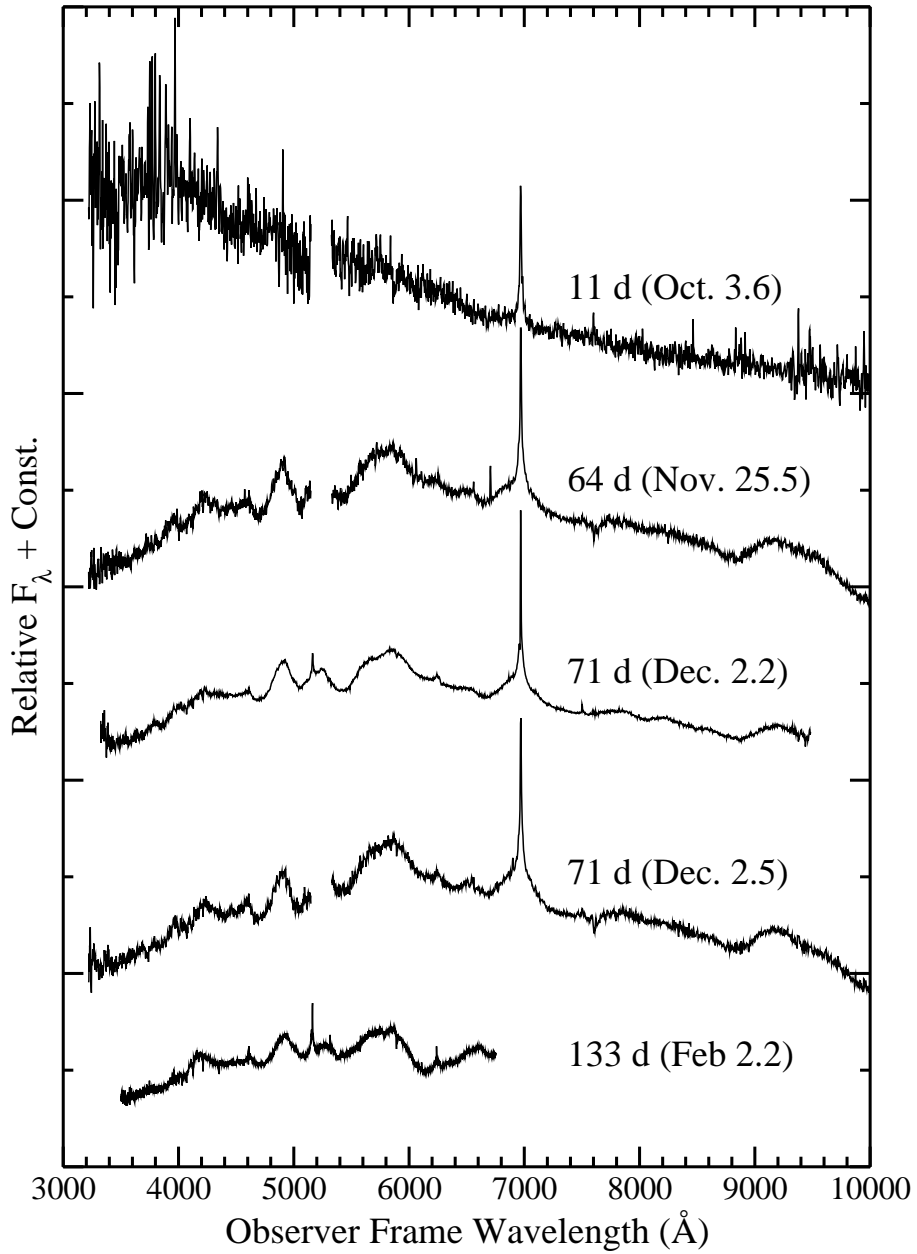


Fig. 2.— Combined spectroscopy of SN 2005gj. The top two spectra were collected with SNIFS, the third with LRIS, the fourth again with SNIFS and the fifth with LRIS on the dates shown. The SNIFS spectrum from December 2.5 is a coaddition of two spectra from the same night. The age of each spectrum with respect to an assumed explosion date of 2005 September 22.6 UTC is shown.

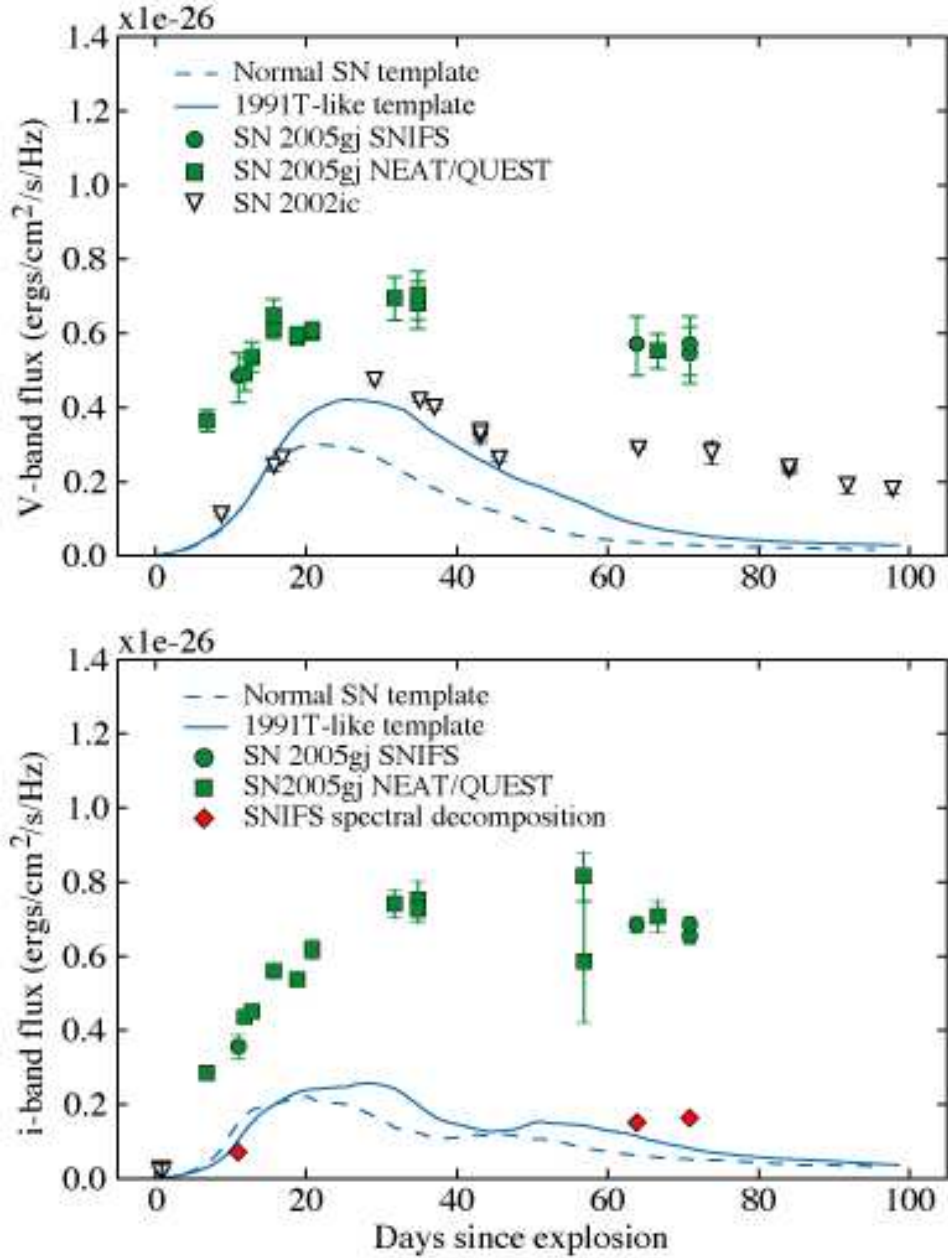


Fig. 3.— Comparison of SN 2005gj and SN 2002ic flux with SN Ia templates in *V*-band (a) and SDSS *i*-band (b). The SN 2005gj *V*-band data are extrapolations from other filters based upon the shape of the SNIFS spectra. The inferred SN Ia flux from a spectral decomposition is shown with red diamonds. To fit these points, the template needs to be brightened by 0.12 mag and either stretched by 1.32 or shifted by 16 days (or a combination thereof).

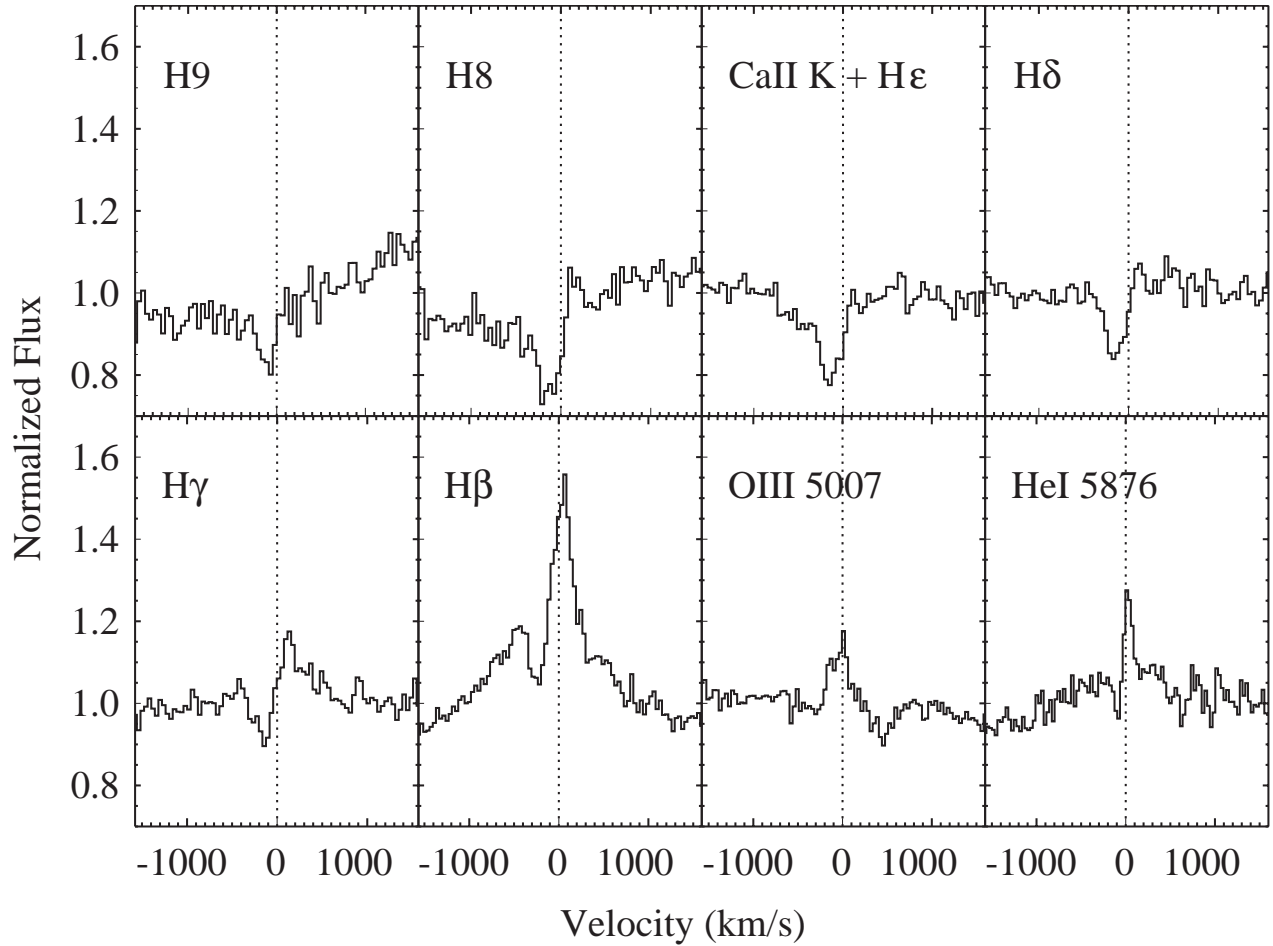


Fig. 4.— Velocity plot for hydrogen Balmer, [O III]  $\lambda$ 5007, and He I  $\lambda$ 5876 lines from the day 133 spectrum obtained with LRIS.

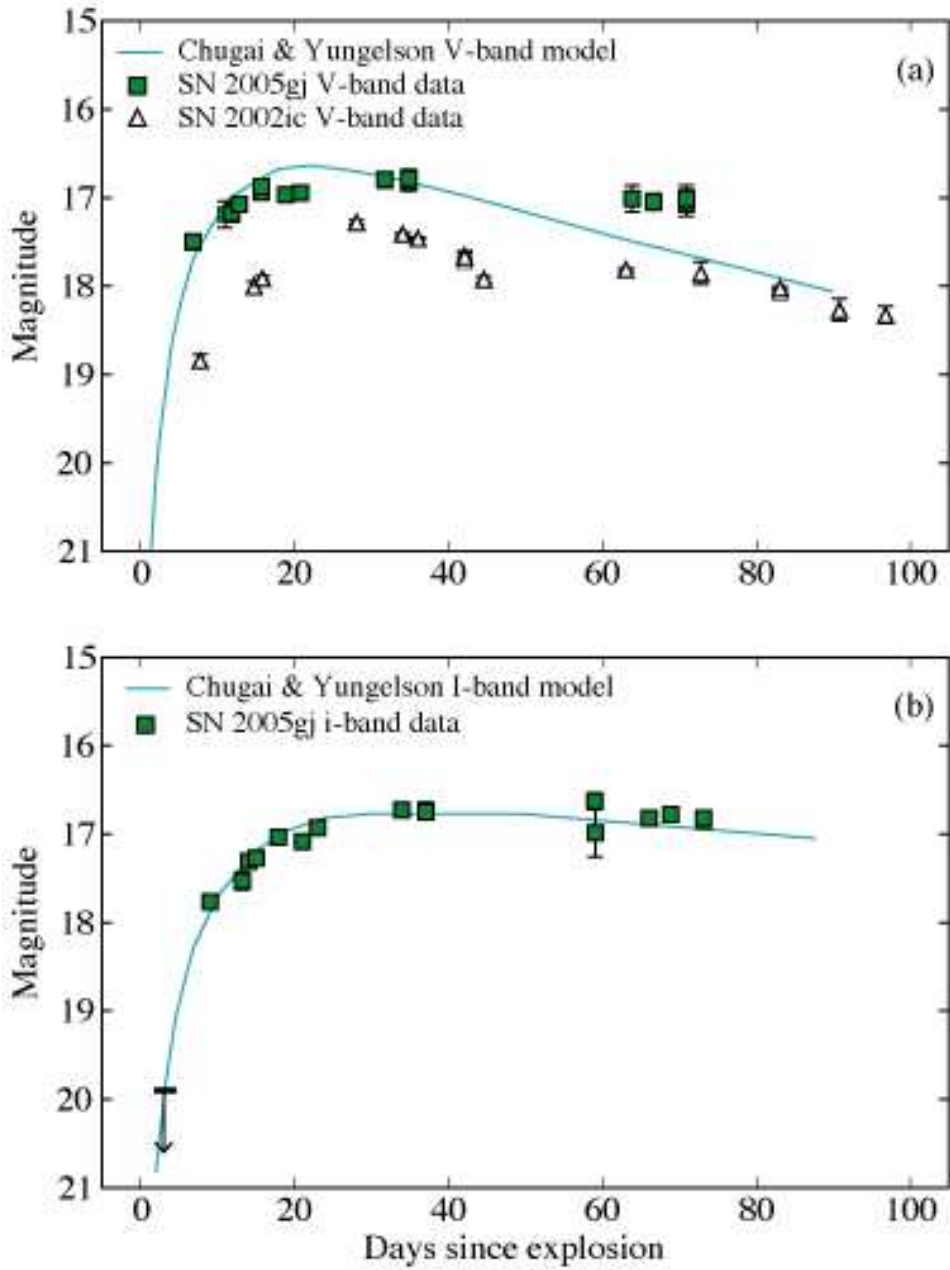


Fig. 5.— Comparison of SN 2005gj data with the  $V$ - and  $I$ -band lightcurve model of Chugai & Yungelson (2004b) as calculated for SN 2002ic using a flat CSM radial density profile. The SN 2005gj  $V$ -band data are extrapolations from other filters based upon the shape of the SNIFS spectra. The magnitudes of the model have been shifted to align with the data and a best fit explosion date of 2005 September 20.4 is used.

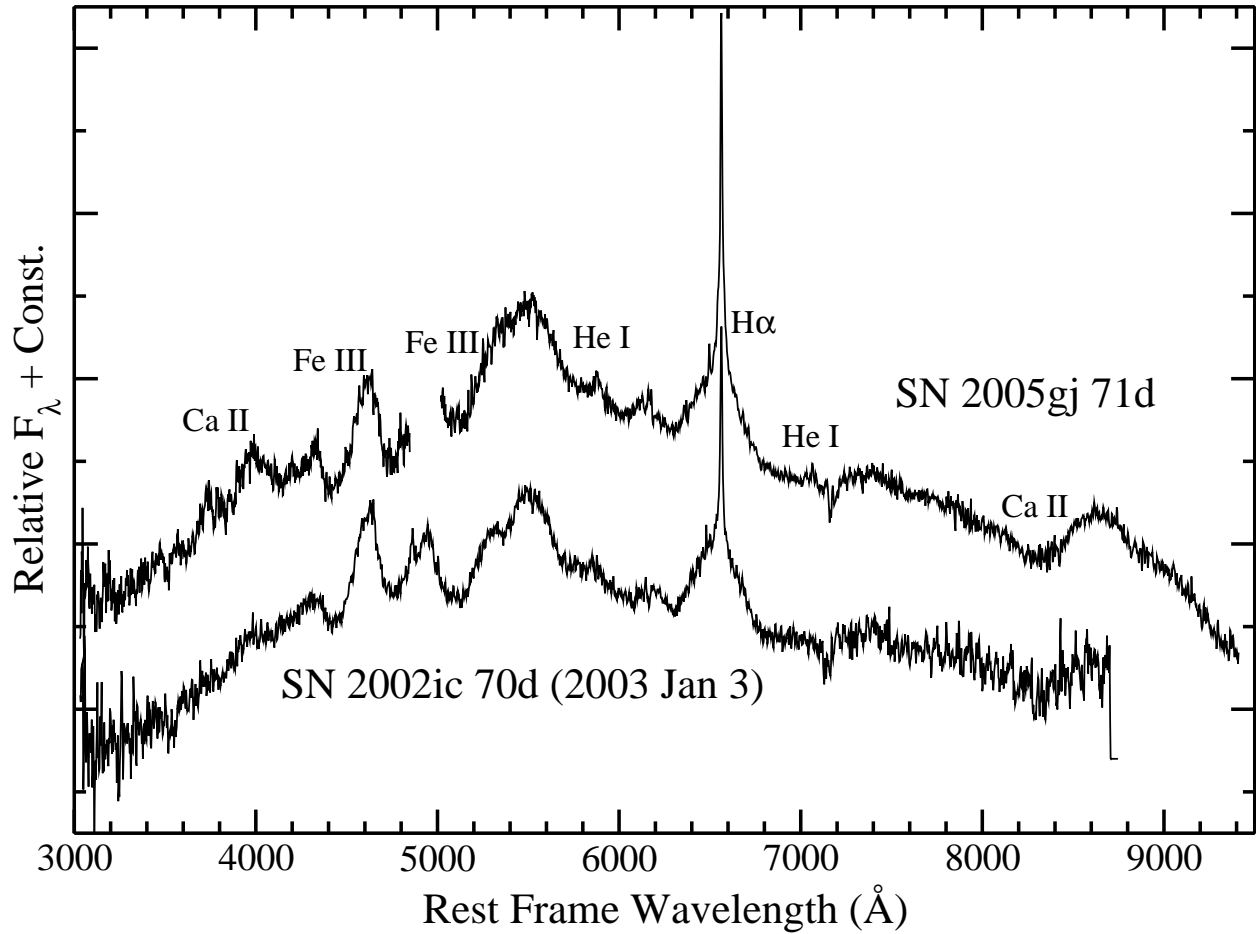


Fig. 6.— Comparison of the spectrum of SN 2005gj 71 days after explosion with that of SN 2002ic at approximately the same phase (assuming an explosion date of 2005 November 5 UTC for SN 2002ic).

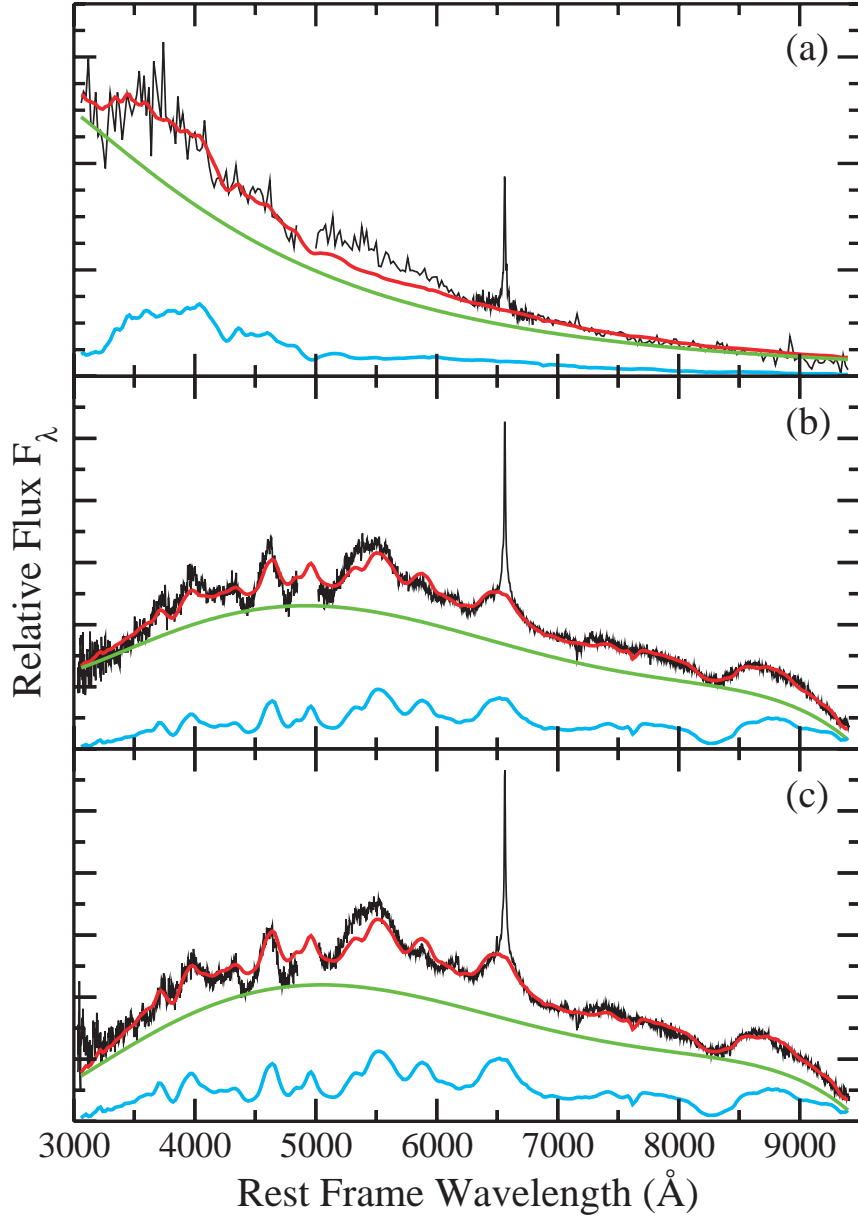


Fig. 7.— Decompositions of the SN 2005gj spectra. Panel (a) compares the spectrum from 11 days after explosion (rebinned outside the H $\alpha$  region for clarity) to a 12,400 K blackbody plus SN 1991T-like template spectrum from the same rest frame phase. Panels (b) and (c) show the decomposition of the day 64 and day 71 spectra in terms of a smooth polynomial plus SN 1991T-like template at 60 and 66 rest frame days after explosion (respectively). In each panel the sum of the two components, and the two individual components, are shown.

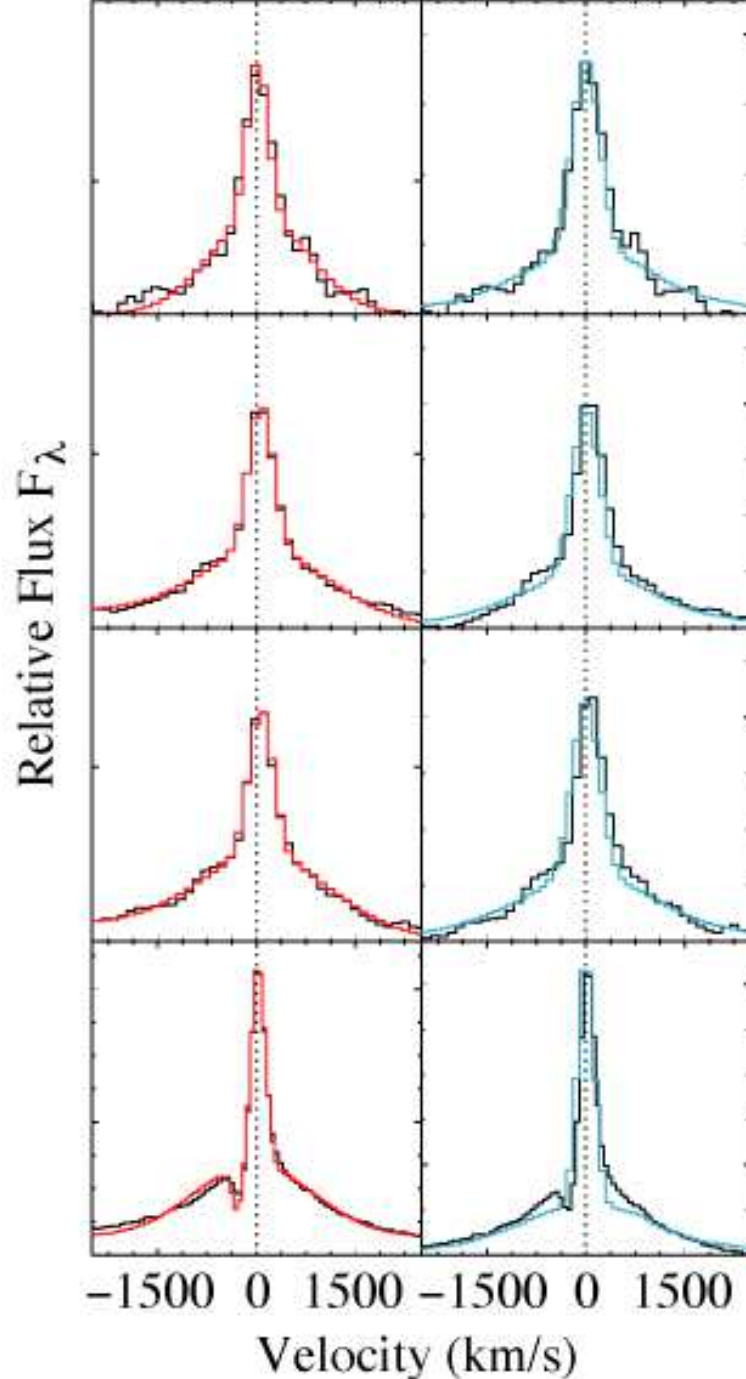


Fig. 8.— SN 2005gj H $\alpha$  line velocity profiles and fits. Each row contains our measurements (black stepped line) on a given day. On the left, a model using two Gaussians (plus a P Cygni profile for the last epoch) is shown (red line). On the right a fit based on a Monte-Carlo electron-scattering simulation is shown. The observations epochs are, from top to bottom, SNIFS day 11, SNIFS day 64, SNIFS day 71 and LRIS day 71.

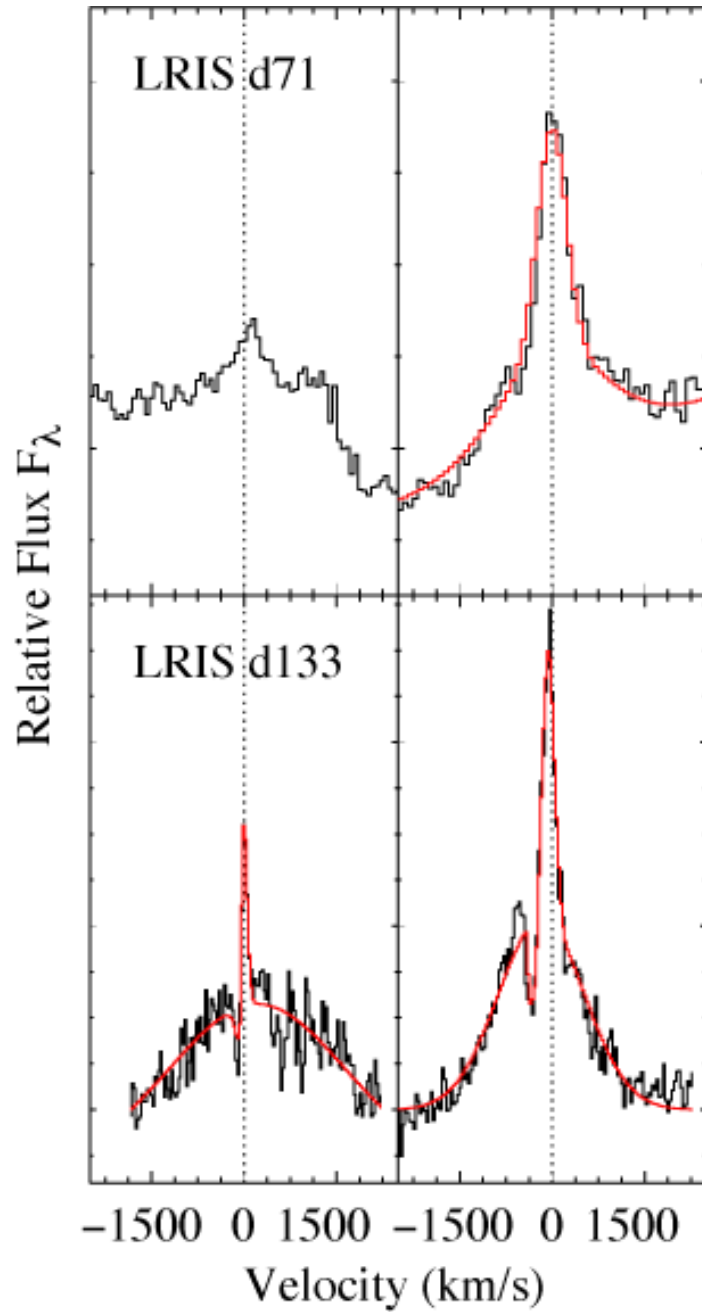


Fig. 9.— He I 5876Å (left) and H $\beta$  (right) line velocity profiles and fits. First row shows LRIS day 71, with the H $\beta$  line modeled as the sum of two Gaussians. Second row: LRIS day 133, with both He I 5876Å and H $\beta$  modeled as the sum of two Gaussians plus a P Cygni profile.

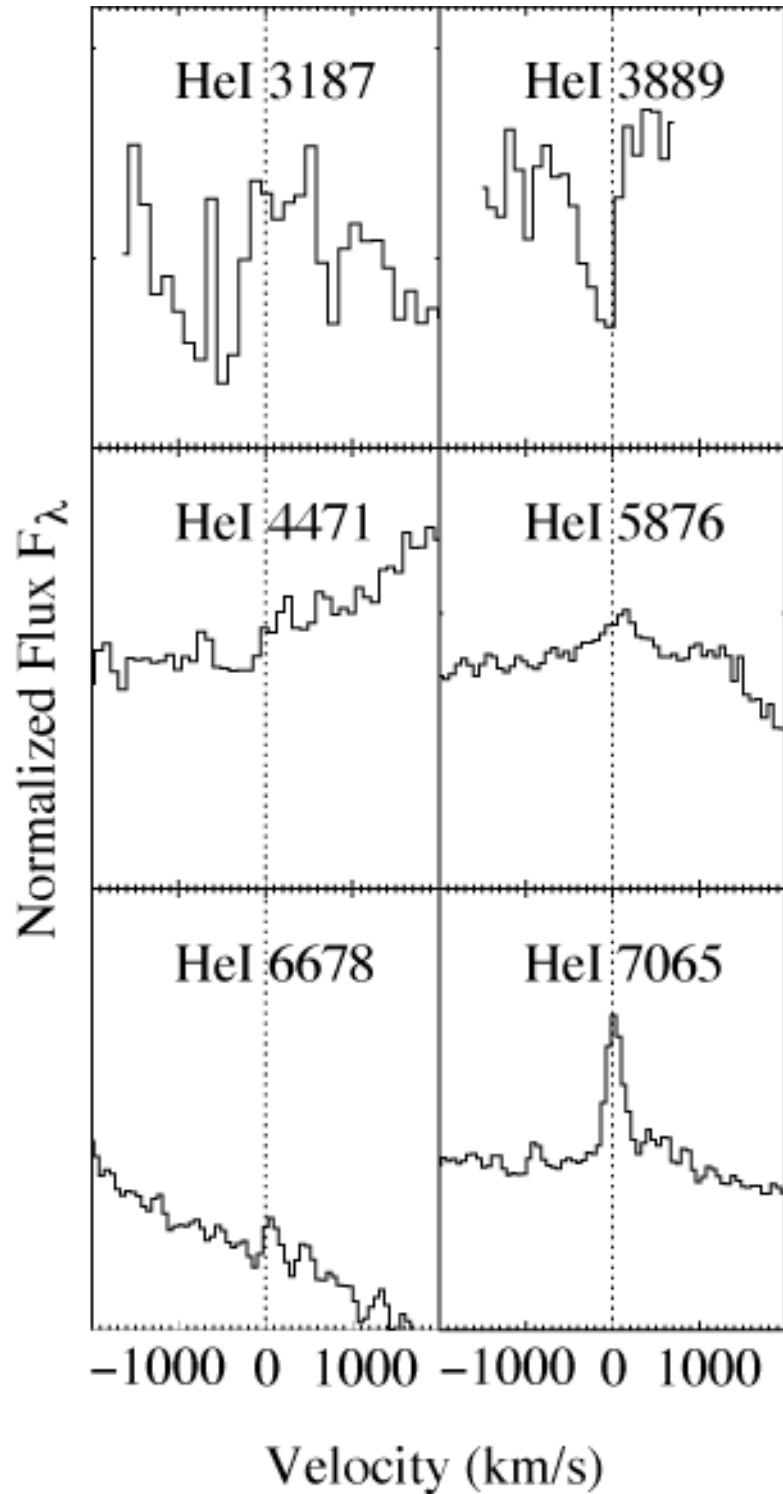


Fig. 10.— Line velocity profiles for He I lines from our day 71 LRIS spectrum. Note that the feature at He I 3889Å is most likely to be the H8 line of the hydrogen Balmer series.

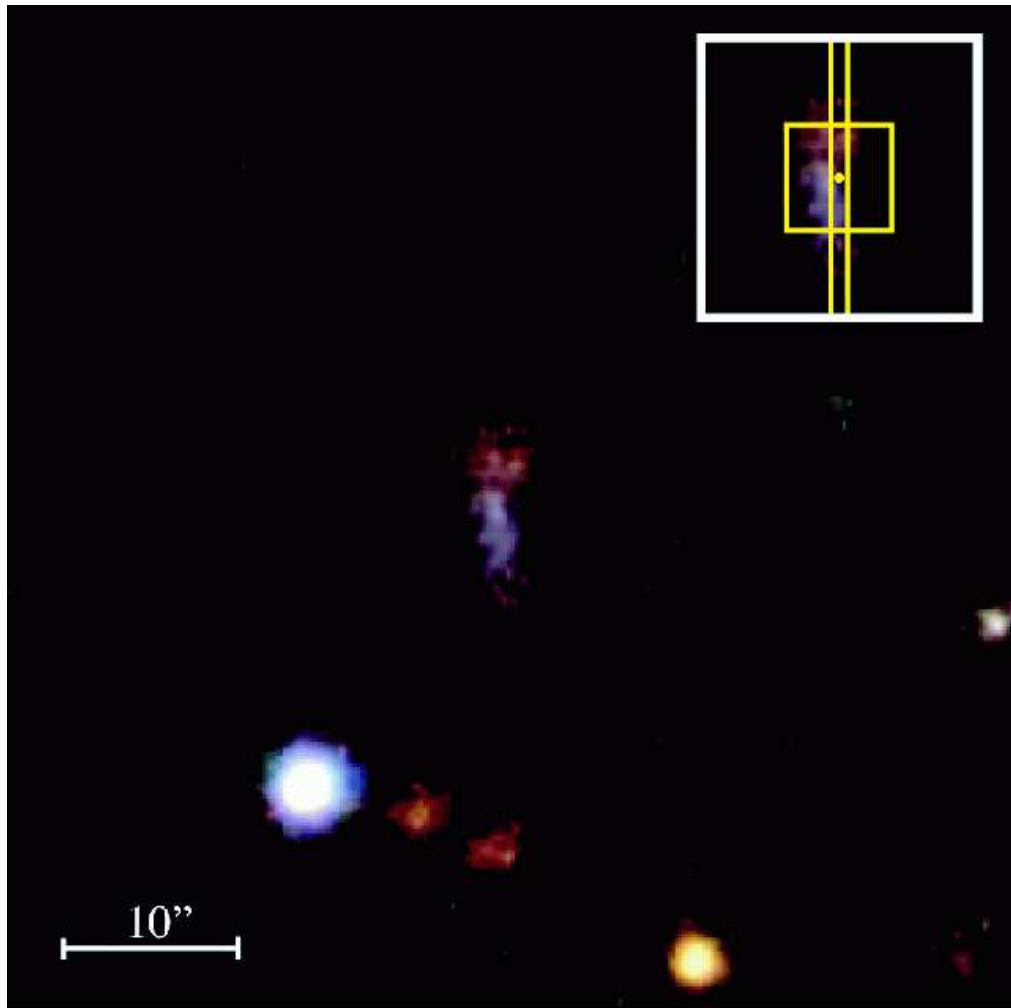


Fig. 11.— SDSS *gri* color composite of the host galaxy of SN 2005gj with north up. In the inset to the upper right, the SNIFS IFU 6x6 arcsecond field of view is shown as a square, the LRIS 1" wide slit runs north and south, and the location of SN 2005gj on the host is indicated by the dot. The bar at the lower left is 10".

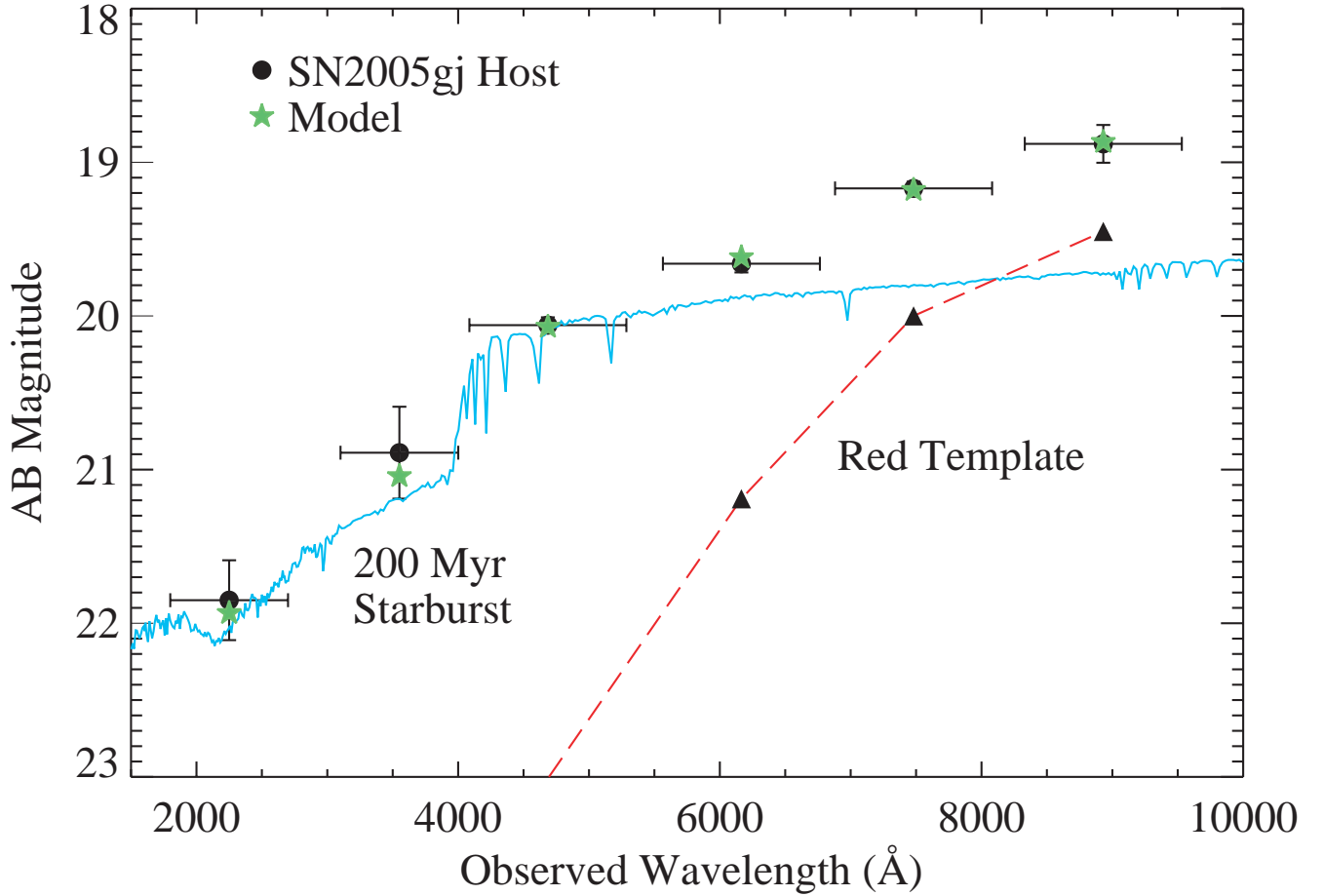


Fig. 12.— Spectrum of the host of SN 2005gj from UV and optical broadband photometry. Each black circle indicates the AB magnitude, uncorrected for extinction, plotted at the mean wavelength, of each photometry point. The error bars in magnitude represent the photometric uncertainties, while the error bars in wavelength give an approximate indication of the wavelength range of each bandpass. Also shown are the components of a fit — the starburst models of Leitherer et al. (1999) plus a red galaxy template taken directly from a galaxy near the host of SN 2005gj. In performing the fits, the starburst models were reddened and then integrated over the detailed filter bandpass. These starburst models were scaled and combined with the red template, and then the resulting model spectrum was scaled to fit the data. The results of the fit are indicated with green star symbols.